





RESEARCH ARTICLE

# Improving the sea state forecasts by using local wave observations and the ensembleBMA software

Tatjana Kokina<sup>1\*</sup> , Daniel Santiago Pelaez-Zapata<sup>1,2</sup> , Thomas Brendan Murphy<sup>1</sup>  and Frédéric Dias<sup>1,2</sup> 

<sup>1</sup>School of Mathematics and Statistics, Earth Institute, University College Dublin, Belfield, Dublin, D04 V1W8, Ireland

<sup>2</sup>Centre Borelli, ENS Paris-Saclay, 91190, Gif-sur-Yvette, France

\*Corresponding author. Email: [tatjana.kokina@ucdconnect.ie](mailto:tatjana.kokina@ucdconnect.ie)

**Received:** day month year; **Revised:** day month year; **Accepted:** day month year

**Keywords:** sea-state forecast; Bayesian Model Averaging; waves; significant wave height; wave statistics

## Abstract

The main goal of this study is to investigate if the publicly available sea state forecasts for the Aran Islands region in the Republic of Ireland can be improved. This improvement is achieved by using the combination of local scale sea state forecasts and Bayesian Model Averaging techniques. The question of a good forecast has been around since the start of forecasting. With current state of the art numerical models, computational power, and vast data availability, we consider if it is possible to improve model forecasts only by using the combination of publicly available forecasts, free open-source software, and very moderate computational power. It is shown that it is possible to improve the sea state forecast by at least 1%, and in some cases up to 8%. The reduction of error is between 6% and 48%. With more careful and specific selection of training parameters it is possible to improve the forecast accuracy even more. The possibility of extending this local improvement to the whole coastal area around the island of Ireland is explored. Unfortunately, it is currently impossible, due to a lack of live data buoys in the coastal waters. Nonetheless it is shown that the proposed process is simple and can be implemented by anyone whose livelihood depends on an accurate sea state forecast. It does not require large computational power, model forecasts are publicly available, and there is minimal to no training in forecasting and statistics required to enable one to perform such improvements for one's area of interest, provided one has access to live wave data.

## Impact Statement

This paper discusses the importance and accessibility of accurate and timely sea state forecast. It serves as a guide for a wider audience that might be interested in improving the accuracy of the local area forecasts.

## 1. Introduction

According to the United Nations Statistics Division, around 600 million people live in coastal areas that are less than 10 m above sea level, while nearly 2.4 billion people (about 40 per cent of the world's population) live within 100 km of the coast (United Nations). Such proximity to the ocean has a great impact on the livelihood of the people – the coastal communities depend on the sea in many aspects, from transportation to sustenance. Providing great benefits, such proximity to the ocean brings great

challenges as well. All the activities and general safety highly depend on the state of the ocean, and ability to forecast the sea state accurately is of paramount importance.

Weather and sea state forecasting has been a subject of interest for more than a century. It is becoming more interesting with the latest extreme weather events brought by changes in the climate (**Monirul Qader Mirza M. [2003]**). One has to be mindful of how difficult it is to produce an accurate weather and sea state forecasts. There are numerous groups of professionals, who work daily on forecasting models to produce accurate forecasts. The number of variables that one needs to account for, the computational expenses, the in-situ measurements, satellite observations illustrate the huge amount of work that is required to produce an accurate forecast. High standard models include the Global Forecast System (GFS), a weather forecast model produced by the National Centers for Environmental Prediction (NCEP); Wavewatch III (WW3) (wind and wave forecast), developed by an international team around NOAA/NCEP and used to forecast marine meteorology by Météo-France (for wave and submersion vigilance), SHOM, NOAA, and Previmer; the Wave Model (WAM); Icosahedral Nonhydrostatic Model (ICON).

In addition to just producing an accurate forecasts, forecast validation and improvement have been long standing questions. Brier and Allen (**Brier G. W., Allen R. A. [1951]**) talk about weather forecast validation being a controversial subject for the last sixty years, and the paper was published in 1951! So it is clear that the question "How good a certain forecast is?" has been out there from the beginning of forecasting.

When talking about forecast evaluation, we need to specify precisely what we are trying to achieve and what the purpose of the verification is. Are we pursuing an economic purpose, for example providing a better meteorological and sea-state forecasts for the fishermen of the Aran Islands, Ireland, or is our purpose purely scientific? Are we just interested in individual model's accuracy? In this article we will present the results of a novel procedure for improving local sea state forecasts by utilising observations from a low-cost buoy (**Raghukumar K., Chang G., Spada F., Jones C., Janssen T., Gans A. [2019]**) and the free open source ensembleBMA software (**Fraley C., Raftery A. E., Gneiting T., Sloughter J. M. [2008]**).

An extensive research project in improving forecast errors and uncertainty was undertaken by UW Probcast Group, resulting in a number of publications. The goals of UW Probcast Group were to develop methods for evaluating the uncertainty of mesoscale meteorological model predictions, and to create methods for the integration and visualization of multi-source information derived from model output, observations and expert knowledge, see **Grimt E. P., Mass C. F. [2002]** for example. A number of questions were addressed by the group, including the uncertainty in forecasts (**Gneiting T., Raftery A. E., Westveld A. H., Goldman T. [2005]**), calibration of forecasts ensembles, model evaluation (**Fuentes M., Raftery A. E. [2005]**), and the work of **Gneiting T., Raftery A. E. [2007]** on proper forecast scoring rules, amongst many other publications.

Work presented in this article was inspired by the work of the UW Probcast Group. However, the original work of the UW Probcast Group focused on atmospheric variables, such as temperature, precipitation, and wind. The work presented in this publication concentrates on improving the sea state forecast. We will use the significant wave height ( $H_s$ ) as a forecast variable that will be improved using the proposed techniques.

Here we will present partial results of the ongoing project Wave Obs, which is part of the HIGH-WAVE project. HIGHWAVE is an interdisciplinary European Research Council ('ERC') project at the frontiers of coastal/ocean engineering, earth system science, statistics and fluid mechanics that explores fundamental open questions in wave breaking. The objectives of the project are primarily to develop an innovative approach to include accurate wave breaking physics into coupled sea state and ocean weather forecasting models, but also to obtain improved criteria for the design of ships and coastal/offshore infrastructure, to quantify erosion by powerful breaking waves, and finally to develop new concepts in wave measurement with improved characterisation of wave breaking using real-time instrumentation. The project includes new approaches to field measurements and breaking wave forecast improvements.

The Wave Obs project develops tools for improved wave forecasts, but at the same time plays a role for the whole project by providing daily forecasts for the team, and a wider audience.

Wave Obs started in January 2020 as an alert service for the project engineer. This alert service was put in place for timely weather warnings and to assist in planning of instrument deployment and maintenance. As mentioned above, HIGHWAVE is an interdisciplinary project that requires extensive instrument deployment and real time data transmission. The physical research station is currently located on Inis Meáin, Aran Islands, place of highly energetic wave events, strong gale force winds, and rapidly changing weather. Hence weather and sea state dependence is a high risk factor for the successful completion of all aims of HIGHWAVE, that requires careful planning.

The original aim of Wave Obs was to provide the daily forecasts from various sources to allow for accurate planning of instrument deployment and maintenance. Wave Obs has developed further, and now comprises of a collection of historical daily of forecasts that are stored on the HIGHWAVE website ([www.highwave-project.eu](http://www.highwave-project.eu)) for the benefit of the team, and local community of the Aran Islands. Additionally a Telegram Bot has been set up, and the same daily forecasts are distributed through Telegram, where any member of public can subscribe to receive daily forecasts, including a short text description and three plots with atmospheric and sea-state variables. Constant strive to improve the provided information has led the authors to the idea of improving the collected forecasts by using Bayesian Model Averaging ('BMA') techniques and providing an improved forecast. A short description of Wave Obs can be found in the Methods section. A more detailed description of particular variables of interest ( $H_s$ ) can be found in the Methods section as well.

The article is structured as follows: in the Methods section we present Wave Obs, observational data collection using weather stations and low-cost buoys, a short overview of the free ensembleBMA software, and basic statistics. In the Results section we present a comparison of raw observation data with the forecasts, and then a comparison of improved forecast with real ocean observations. In the Discussion section we share our views on the possibility of extending the improved forecasts to a global scale, and discuss possible extensions to the improved forecast.

## 2. Methods

### 2.1. Wave Obs

Originally Wave Obs started as a warning tool for the HIGHWAVE project engineer based on the West Coast of Ireland. As the wider HIGHWAVE project requires instrument deployment in the field, weather plays an important role in planning the deployment of instruments. Wave Obs has developed and evolved into an intricate collection of forecasts from various sources, and includes not only wind and wave forecasts, but many more variables, such as temperature, atmospheric pressure, solar radiation. Initially, Wave Obs was a manual task. On a daily basis, the forecasts for the next three days was collected from the different sources, then the forecasts were passed to the interested parties, and a database was populated manually. The forecast collection process was automated in May 2020. A Python application was developed to automatically download, process, and distribute the forecast data from the different sources. This application extracts a number of sea state and meteorological variables for several locations around the Aran Islands region (Figure 1), accessing the servers of the forecasts data providers through different API protocols.

Considering that all data providers deliver their data in a numerous kind of formats and specifications, a process of data cleaning and transformation into an uniform format is applied and then the data is stored locally using a JSON (JavaScript Object Notation) file format. Each file contains the forecast for five consecutive days and it is stored following the name convention given by the current date. The automation process is carried out by Github workflows and includes two basic steps: first, data is stored in the Google Drive cloud servers on a daily basis, and second, using a Telegram bot, a daily digest on the marine weather forecast contrasting different sources, is automatically sent to a Telegram channel, making it available for the Aran Islands local community (see Wave Obs pipeline in Figure 2).

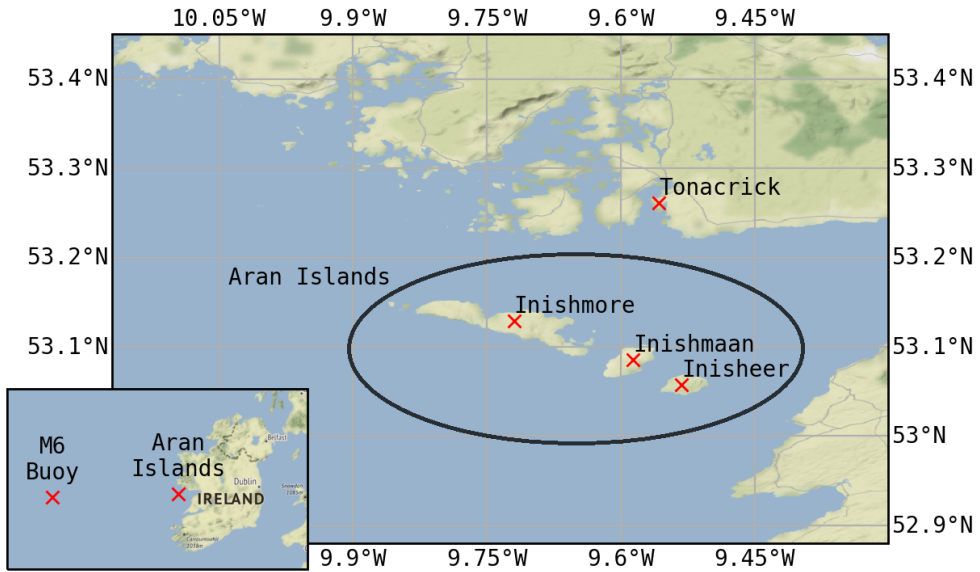


**Figure 1.** Locations (marked with red X) of the points where the forecasts are obtained for.

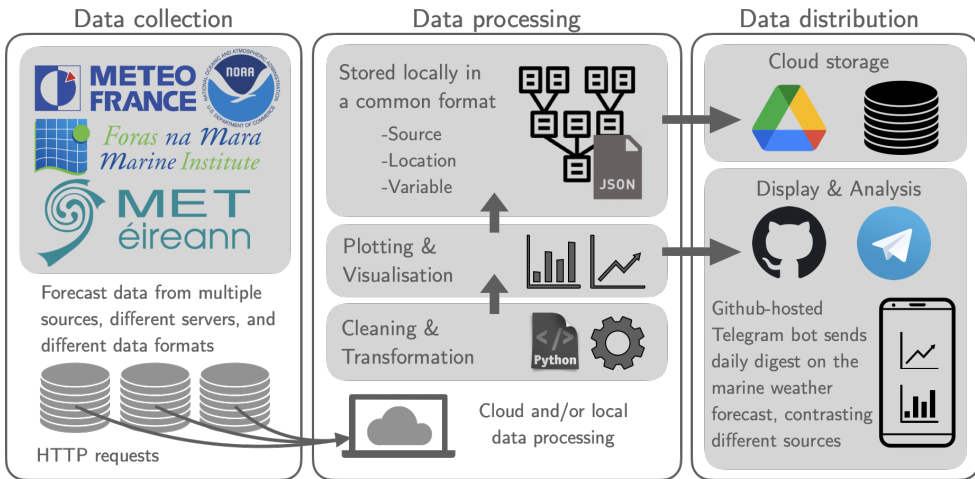


**Figure 2.** Wave Obs pipeline showing a brief description of the data collection, processing and distribution.

In the development of the project, it was established that many agencies that provide forecasts draw the actual information from just a handful of sources. Hence it was decided to only track 'original' sources. As this article concentrates on wave forecasts and measurements we list the wave information forecasts only.

### 2.1.1. Sources

As mentioned above, only four sources are considered for forecast collection. A brief description of each source is presented below.

- *Marine Institute (Ireland)*: The numerical wave model, SWAN, simulates surface gravity waves for a domain covering Irish waters at a resolution of  $0.025^\circ$  (approximately 1.5 km). The model uses Global NCEP GFS for wind forcing and FNMOC WW3 data for the wave boundary conditions. A daily 6 day forecast is generated for wave parameters such as  $H_s$ , swell wave height, mean wave period and mean wave direction. The Marine Institute provides their data through the THREDDS and ERDDAP protocols. The latter is used to access the data using the Wave Obs application. We will denote the Marine Institute as 'MI' in the figures and tables that follow.
- *NOAA WAVEWATCH III Global*: Well established and widely used model with spatial resolution  $0.25^\circ$ , and temporal resolution of 1 h. This is a global forecast issued by NOAA/NCEP. WAVEWATCH III, alike SWAN, solves the random phase spectral action density balance equation for wavenumber-direction spectra. The forecast data is officially delivered using an ERDDAP servers. NOAA/NCEP WAVEWATCH III data is the most comprehensive forecast, it includes wind speed and direction, and main wave sea state parameters (wave height, mean period and direction) for the three main spectral partitions (wind waves, primary and secondary swells). We will denote NOAA WAVEWATCH III Global as 'WW3' in the figures and tables that follow.
- *Météo-France Wave Model (MFWAM) Global Forecast*: The operational global ocean analysis and forecast system of Météo-France with a spatial resolution of  $1/12^\circ$  and a temporal resolution of 3 h provides daily analysis and 5 day forecast for the global ocean sea surface waves. Météo-France uses an implementation of the third generation spectral wave model WAM (**The Wamdi Group** [1988]). This product includes 3-hourly instantaneous fields of integrated wave parameters from the total spectrum ( $H_s$ , period, direction, Stokes drift, and others), as well as the following partitions: the wind wave, the primary and secondary swell waves. We will denote Météo-France Wave Model (MFWAM) Global as 'MF' in the figures and tables that follow.
- *DWD Wave Model Global*: This forecast model, alike MF, uses the generation wave model WAM (**The Wamdi Group** [1988]). This forecast is issued by the German Weather Service (DWD). A global domain with spatial resolution of  $0.25^\circ$  and temporal resolution of 3 h are used. The wind forcing is obtained from the ICON modelling framework, which is a joint project between the German Weather Service and the Max Planck Institute for Meteorology. We will denote DWD Wave Model Global as 'DWD' in the figures and tables that follow.

As HIGHWAVE experiments take place on the West Coast of Ireland, and the Mobile Research Station ('MRS') is currently located on Inis Meáin, one of the Aran Islands, daily forecasts were made available to the local island community. This was achieved by posting daily a 5 day forecasts on the HIGHWAVE website (see examples in Figures 3 and 4). Same forecasts are delivered through a Telegram channel to anyone who has subscribed to it. It is accompanied by a short text description of the weather and sea state expected in the next five days.

In addition to the graphs, a database containing the daily forecasts collection has been developed. Data from this database will be used to validate and train the new improved forecast.

## 2.2. Observational Data Collection

The main goal being an improvement of the forecasts in the future, it is desirable to validate the forecasts in order to determine the accuracy of the available forecasts. To achieve that, a weather station was installed for the validation of atmospheric variables. To establish the accuracy of the sea state forecast two low-cost buoys were deployed in the area of interest. Since we are interested in the sea state forecast, we will only present data collection process from the buoys and not from the weather station.

### 2.2.1. Buoys

As part of the HIGHWAVE project two Spotter buoys were purchased. They were named Wanderer and Explorer. With these two buoys three campaigns were completed:

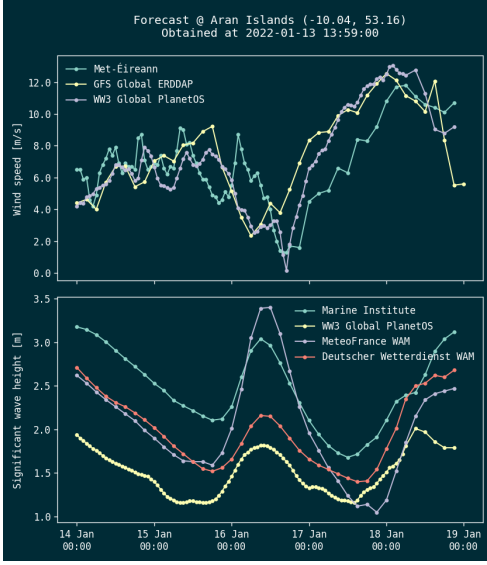


**Figure 3.** Wind and wave forecast example.

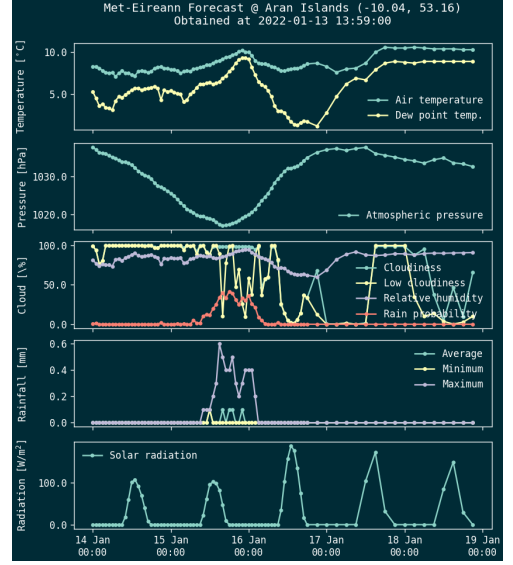


**Figure 4.** Atmospheric variables forecast.

- Wanderer first mission - 1 June 2020 to 19 September 2020
- Explorer first mission - 11 August 2020 - 5 September 2020
- Explorer first mission - adrift - 5 September 2020 - 1 October 2020
- Wanderer second mission - 7 November 2020 - 3 March 2021

The data of interest can be obtained by the software on board of the buoys, either in real-time through satellite connection or directly from the SD card after recovery of the buoy. The downside of using the pre-processed data, in general, is that the on-board algorithms are a ‘black-box’ as such, and the end user is not aware of how the  $H_s$ , for example, is calculated. The following variables are recorded by the Spotter buoys:

- $H_s$ , for all practical purposes:

$$H_s \approx 4\sqrt{m_0}$$

where  $m_0$  is the zeroth-order moment of the variance density spectrum  $E(f)$ . In the wave mode the  $H_s$  is estimated from the zeroth-order moment of wave spectrum ([Sofar Ocean Technologies \[2022\]](#)).

- Mean Wave Period ( $\bar{T}_0$ ) and Peak Wave Period ( $T_p$ ), where the mean period is the variance-weighted mean period ( $T_{m_01}$ ), and the Peak Period is the period associated with the peak of the wave spectrum.
- Mean ( $\bar{\theta}$ ) and Peak ( $\theta_p$ ) Directions. One can define the peak direction  $\theta_p$  as the direction corresponding to the most energetic wave component. It is calculated in terms of the circular moments or Fourier coefficients  $a_1(f)$  and  $b_1(f)$  which are the result of the cross-spectral analysis of the wave-induced horizontal wave displacement and surface elevation ( $x$ ,  $y$  and  $z$ , respectively) as shown by [Kuik A. J., van Vledder G. Ph., Holthuijsen L. H. \[1988\]](#). The exact definitions of both peak wave direction and mean direction are:

$$\theta_p = \tan^{-1} \left\{ \frac{b_1(f_p)}{a_1(f_p)} \right\},$$

and

$$\bar{\theta} = \tan^{-1} \left\{ \frac{\overline{b_1}}{\overline{a_1}} \right\}$$

respectively, where the overbar indicates energy-weighted averaged quantities.

- Other wave parameters, including mean and peak directional spreading.

In this article, we only concentrate on  $H_s$ . The comparison between the Spotter recorded data and forecasts from various agencies is presented in the results section (Section 3).

### 2.3. Statistics

In order to evaluate the accuracy of the individual forecast and the ‘trained’ ensemble forecast, we use the mean absolute error (‘MAE’), mean absolute percentage error (‘MAPE’) in some instances, and the continuous rank probability score (‘CRPS’). In addition, individual weights of each forecast, contributing to the ensemble forecasts, were monitored.

Let  $y_i$  is the observed value,  $f_i$  be a point forecast and  $F_i$  be the probabilistic forecast for each observation  $i = 1, 2, \dots, n$ . MAE, MAPE, and CRPS can be calculated using the model forecasts and observations, as per equations (1)–(3), or using the built in functions in the ensembleBMA software. These three measures were selected to evaluate the performance of individual, adjusted, and ensemble forecasts, as they are widely used in measuring the performance for probabilistic forecasts. In addition, MAE and CRPS were used to estimate the optimal training window for each buoy.

The mean absolute error is given by:

$$\text{MAE} = \frac{\sum_{i=1}^n |y_i - f_i|}{n}. \quad (1)$$

The MAPE, is similar to MAE, and is given by:

$$\text{MAPE} = \frac{1}{n} \sum_{i=1}^n \frac{|y_i - f_i|}{|y_i|}. \quad (2)$$

The continuous rank probability score is widely used to assess the accuracy of probabilistic forecasts [eg. **Gneiting T., Raftery A. E., 2007**]. Let  $F_i$  be the cumulative distribution function of the probabilistic forecast for observation  $i$ , then the continuous rank probability score is given as:

$$\text{crps}(F_i, y_i) = \int_{-\infty}^{\infty} (F_i(x) - H(x - y_i))^2 dx,$$

where  $H$  is the Heaviside step function. The mean continuous rank probability score (‘CRPS’) score is given as the average score over all instances:

$$\text{CRPS} = \frac{1}{n} \sum_{i=1}^n \text{crps}(F_i, y_i). \quad (3)$$

The value of the weight of individual forecast indicates how much the individual model contributes to the ensemble forecast. By evaluating the weight of each individual contribution of forecast, it is possible to exclude forecasts that have no or little contribution to the ensemble. However, in the results presented here, we did not exclude low weighting forecasts from the ensemble forecasts.

#### 2.4. Bias corrected forecasts

In the process of producing the ensemble averaged forecast, individual forecast models are first bias-corrected [**Gneiting T., Raftery A. E., Westveld A. H., Goldman T., 2005, Sloughter J. M., Gneiting T., Raftery A. E., 2013**]. There are various ways of performing this process. We briefly describe how such a bias-correction is completed in the ensembleBMA software.

Let  $y_i$  be the observed value and let  $f_i$  be the point forecast for observation  $i = 1, 2, \dots, n$ . A simple linear model is used to model the relationship between the forecast and the observed values. That is,

$$y_i = a + b f_i + \epsilon_i,$$

where  $\epsilon_i \sim N(0, \sigma^2)$ . The linear model is fitted using least squares to yield parameter estimates  $\hat{a}$  and  $\hat{b}$ . The bias corrected forecasts are then given as

$$\hat{f}_i = \hat{a} + \hat{b} f_i;$$

the estimates  $\hat{a}$  and  $\hat{b}$  determine how much the forecast needs to be shifted and scaled in the bias correction process. Furthermore, the linear model gives a probabilistic individual forecast, where

$$Y_i | f_i \sim N(a + b f_i, \sigma^2). \quad (4)$$

In practice, the bias-correction process is fitted to a time window of  $m$  observations and it is then applied to forecasts immediately after the time window.

#### 2.5. Bayesian Model Averaging techniques

The forecasting process used to be a deterministic one. It was believed that if you initialised your model with most accurate input information, you would produce the most accurate forecast. However, with advances in high performance computing and available resources, ensemble forecasts became available. An ensemble forecast is one that would consist of a number of numerical models outputs, with slightly perturbed initial conditions. For a comprehensive overview of ensemble forecasting, we refer the reader to **Gneiting T., Raftery A. E. [2015]**. In essence, the ensemble forecasts are probabilistic ones, and even though both deterministic and probabilistic forecasting is trying to predict a certain 'event', the actual error or uncertainty can only be found in the probabilistic forecast. There are of course errors present in the ensemble forecasts as well. However, it has been shown by **Gneiting T., Raftery A. E., Westveld A. H., Goldman T. [2005]** that it is possible to improve the ensemble forecasts by applying some post-processing based on Bayesian model averaging ('BMA') techniques.

The essence of the BMA idea is in combining not the outcome of different initial conditions for one model, but rather different models. Properly introduced in late seventies by **Leamer E. E. [1978]**, it did not get much attention till the nineties (**Kass R. E., Raftery A. E. [1995]**), see a comprehensive review in **Hoeting J. A., Madigan D., Raftery A. E., Volinsky C. T. [1999]**, for example. We will not try to re-explain here the whole theoretical background for the BMA technique but will merely give the reader the basic idea.

The BMA forecasting model is based around taking a weighted combination of individual forecasting models. Suppose, we have  $K$  bias-corrected individual forecasting models (see Section 2.4), then the BMA forecast is based on (4) is given as

$$Y_i | f_{1i}, f_{2i}, \dots, f_{Ki} \sim \sum_{k=1}^K w_k N(a_k + b_k f_{ki}, \sigma^2). \quad (5)$$



The unknown parameters are estimated using an expectation-maximization (EM) algorithm [Dempster A. P., Laird N. M., Rubin D. B., 1977] and the details of this are given in [Gneiting T., Raftery A. E., Westveld A. H., Goldman T., 2005, Section 2b].

A point forecast of  $Y_i$  from the BMA model is thus given as

$$\hat{y}_i = E(Y_i | f_{1i}, f_{2i}, \dots, f_{Ki}) = \sum_{k=1}^K w_k (a_k + b_k f_{ki}),$$

which is a weighted average of the bias-corrected individual forecasts. In practice, the weights are also estimated using an  $m$  observation time window and used for subsequent forecasts.

Thus, in BMA, rather than concentrating on the various outputs of one selected model, a number of different models are considered, determined by the estimated weights  $\hat{w}_1, \hat{w}_2, \dots, \hat{w}_K$ . As shown below (Section 3.3.1), it is possible, and is the case, that one model outperforms another for a short period of forecasting, with the original model performing better again later. In the case of sea state forecast, it can be as simple as one model being better at predicting calm summer seas, and another being more accurate in the winter. We present below the evidence of one model outperforming another in different conditions.

### 2.5.1. Data distribution normality assumption

The proposed method, as outlined in Section 2.4 and Section 2.5 is based on a normality assumption for the difference between the adjusted forecast and the observed significant wave height (see equations (4) and (5)). The proposed BMA technique, based on the normality assumption, has also been successfully used in previous studies for sea level air pressure and temperature forecasting (Raftery A. E., Gneiting T., Balabdaoui F., Polakowski M. [2005]). However, there also exist BMA techniques based on non-normal distributions (Sloughter J.M., Raftery A.E., Gneiting T., Fraley C. [2007]) which have been successfully used for precipitation forecasts.

We investigated the use of using the BMA approach with other distributional assumptions (eg. gamma distribution) but we found that the results were less accurate than the approach based on the normal distribution.

We investigated the normality assumption by comparing the observed significant wave height to the bias-adjusted forecasts using histograms and QQ-plots, see figures 5 and 6 for the M6 winter adjusted forecasts (all other missions are provided in the supplementary material). The results showed that the normality assumption held approximately, but some extreme differences were observed that are not well accommodated by the normal distribution. This suggests that an extension of the proposed approach could be developed using heavy tailed distributions to accommodate these large differences.

## 3. Results

### 3.1. Forecasts vs buoy observations

As mentioned in the Methods section, we present here 'brute force' comparison between the forecasts of interest and record from Spotter buoy campaigns. As part of Wave Obs we have been collecting 3 day forecasts until December/January 2020, and 5 day forecasts since January 2021. However, in this paper we concentrate on 24, 48 and 72 h forecasts, denoted 24H, 48H, and 72H in the plots and tables. In figure 7 we present the 24, 48, and 72 h forecasts and the real data from the Wanderer first mission. Similar comparison is presented for the first Explorer and second Wanderer missions in the Supplementary material, see figures 33 and 34.

As one would expect, the forecasts are quite reasonable, and predict the  $H_s$  quite well. However, the further away is the forecast from the forecast date, the less accurate it is, which is not surprising. In table 1 we present the MAE for individual models, depending on the forecast hour. As mentioned

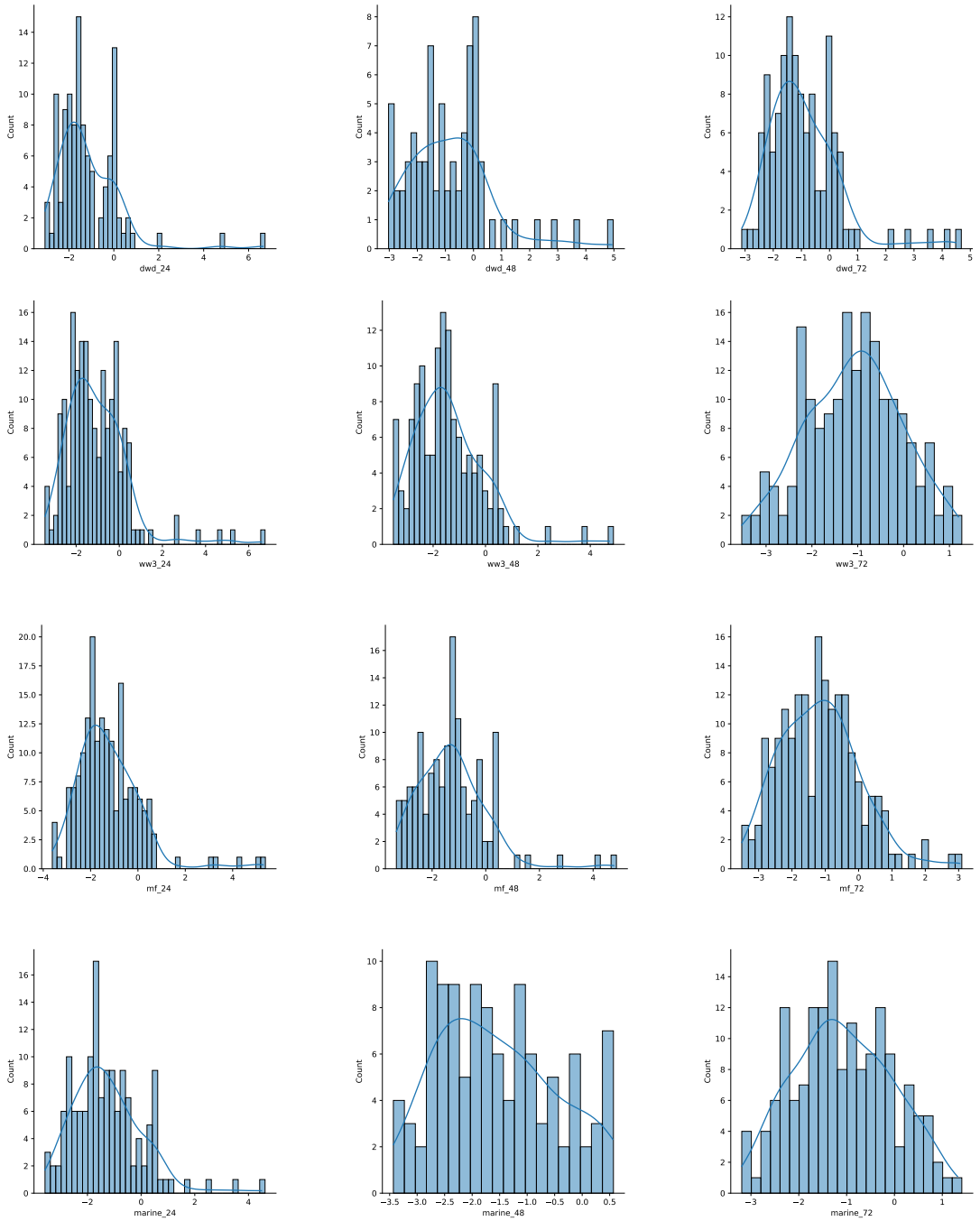


**Figure 5.** Histograms of the difference between the adjusted forecasts for M6 winter period versus the actual observed value. From top to bottom: DWD, WW3, MF, Marine Institute. From left to right: 24H, 48H, 72H.

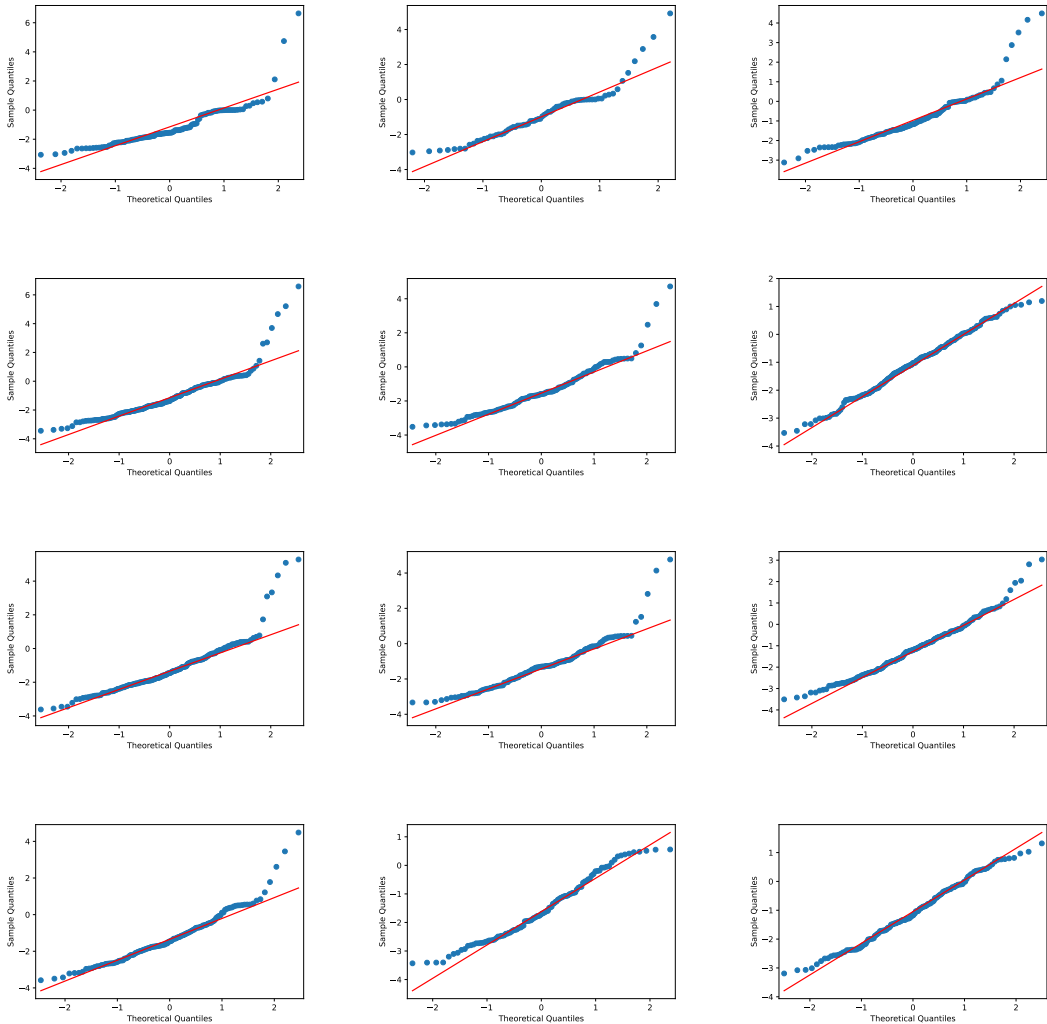


**Figure 6.** *Q-Q plots of the difference between the adjusted forecast for M6 winter period versus the actual observed value. From top to bottom: DWD, WW3, MF, Marine Institute, from left to right: 24H, 48H, 72H.*

above, the MAE values confirm that the 24 h forecast is the most accurate one. We present results for all missions and all model forecasts.

We would like to point out that the previous statement regarding the accuracy of the forecast that decreases with a longer time lag is still true for the DWD. However, the WW3 and MF models do not follow the same behaviour. Overall, for the period covered, the best accuracy shifts to either 48 h or even 72 h forecasts at some stage, or matches the accuracy of the 24 h forecast.

Similar results are presented in the Supplementary materials, figures 33 and 34 for the first Explorer and second Wanderer missions. The period covered is between June 2020 and early March 2021. This period, which included calm summer seas and rough winter seas, can be considered versatile enough for the forecast training purposes. [The interannual variability is a valid concern point that can be raised.](#) [The long term variability of wave climate and extreme wave events particularly at the Irish coast, North](#)

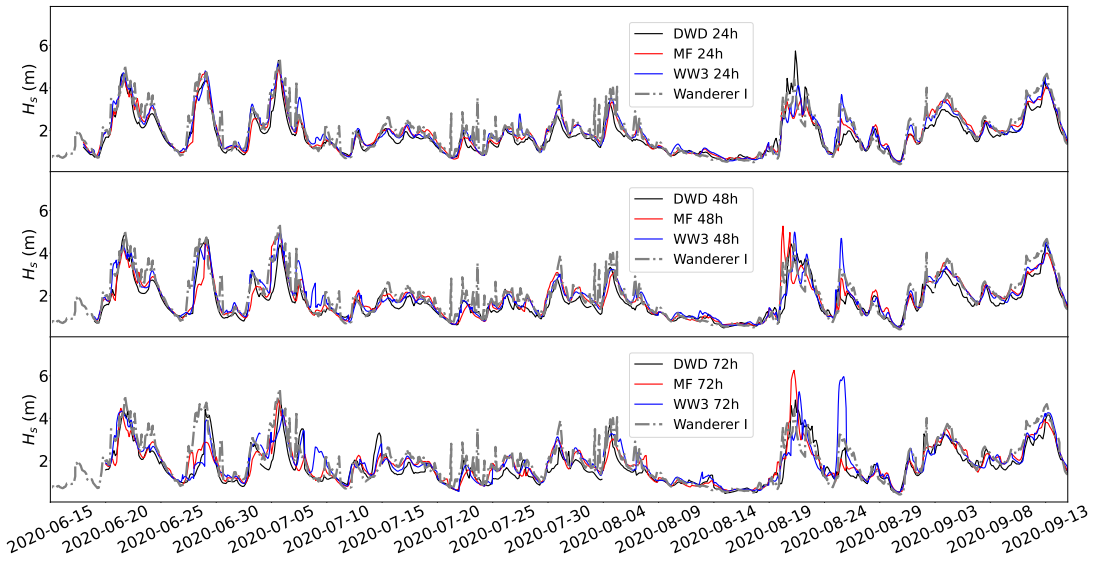


**Figure 7.** Comparing actual recorded  $H_s$  to the 24 h (top), 48 h (middle), and 72 h (bottom) forecasts of the  $H_s$  for the first Wanderer mission.

Atlantic, and the Bay of Biscay, have been a topic of number of recent studies. However, an overall message is that for the period 1979–2012 at least there were no significant trends for the mean up to the 99th percentile of significant wave height, with the caveat that climate trends are very hard to differentiate from low frequency variability in the climate system. For the comprehensive review of studies regarding wave climate trends, we would refer the reader to [Gallagher S., Tiron R., Dias F. \[2014\]](#), [Gallagher S., Gleeson E., Tiron R., McGrath R., Dias F. \[2016\]](#).

The total observational period with the Spotter buoys was between June 2020 and early March 2021, and for the M6 location the authors looked at summer 21 June 2020 – September 2020, and separately for 20 October 2021 – 20 November 2021. Same process of forecast improvement was carried out for the period between June 2020 and March 2021 for the Spotter buoy in retrospect. In other words, we produced a daily ensemble forecast for this period, and compared it to the actual observations. Hence, we believe that seasonality was taken into consideration in the training process. These retrospect forecasts are not presented for the sake of brevity.

The months of April and May were not included, hence the whole year was not covered. But this should not be an issue due to the training period selected. For the three missions (Explorer I, Wanderer I, and Wanderer II) the sliding training period was 5, 10, and 20 days respectively. Even at the maximum

**Table 1.** Average mean absolute error (in meters) of individual forecasting models, depending on the forecast time for Explorer I, Wanderer I, and Wanderer II missions.

Mission	24H			48H			72H		
	DWD	WW3	MF	DWD	WW3	MF	DWD	WW3	MF
Explorer I	0.58	1.23	0.55	0.77	1.27	0.82	1.01	1.29	1.01
Wanderer I	1.03	1.07	1.03	1.04	1.06 <sup>1</sup>	1.06	1.05	1.06 <sup>1</sup>	1.03 <sup>2</sup>
Wanderer II	1.49	1.86	1.64	1.65	1.95	1.76	1.73	1.85 <sup>1</sup>	1.62 <sup>1</sup>

<sup>1</sup>Note the improved accuracy of either 48H or 72H forecasts.

<sup>2</sup>Note the accuracy of the 72H matching the 24H accuracy

\*The graphs reflecting the difference between the first Explorer and second Wanderer missions are provided in the supplementary material.

training period of 20 days, the window is a sliding window, hence the changing conditions are being captured by the training period, as the forecast develops in time.

As previously mentioned months of April and May have not been part of the forecast improvement period. Even though a number of unusual weather events tend to occur in Ireland during the month of April, on most occasions these events are heatwaves, or extreme rainfall events - but not marine heatwaves that would affect the whole oceanic ecosystem including wave heights.

Overall, we are confident, that since the training window is not fixed, and is of a sliding nature, any variability that might affect the forecast will be captured during the training period, as it moves together with the improved forecast. However, the subject of training windows will be addressed separately.

Taking into account Explorer drifting period, and the period of change of the data collection algorithm, from here, we will only present results of the first Wanderer mission. Results from the two other missions are available in the supplementary material.

Before any forecast training could begin, the optimal training window had to be established. Adopting the approach described in [Raftery A. E., Gneiting T., Balabdaoui F., Polakowski M. \[2005\]](#), a sliding window of length  $m$  (number of days) was chosen.

To select the right value for  $m$ , a number of factors need to be considered. One would expect that the longer the training window, the better the training process would be. However, with longer periods, one might end up with accumulating forecast errors for longer. In addition, the behaviour of ocean waves is not as uniform as that of temperature. For example, one would expect temperatures to stay within average summer values during the month of June and July. Ocean waves, however, are known to have rapidly changing patterns, and for that reason, one would prefer to have a short training period, one capable of adapting quickly to changing conditions. During the selection process, authors looked at MAE and CRPS with a range of values for  $m$  from 5 to 90 days.

In figure 8 we present the evolution of the MAE and CRPS, depending on the number of training days selected. Similar plots are presented in the Supplementary material for the Explorer I and Wanderer II missions in figure 35. From figure 8 it is clear that at some point extending the training window will no longer improve the accuracy: the values of MAE and CRPS plateau. Similar observations can be found in [Gneiting T., Raftery A. E., Westveld A. H., Goldman T. \[2005\]](#).

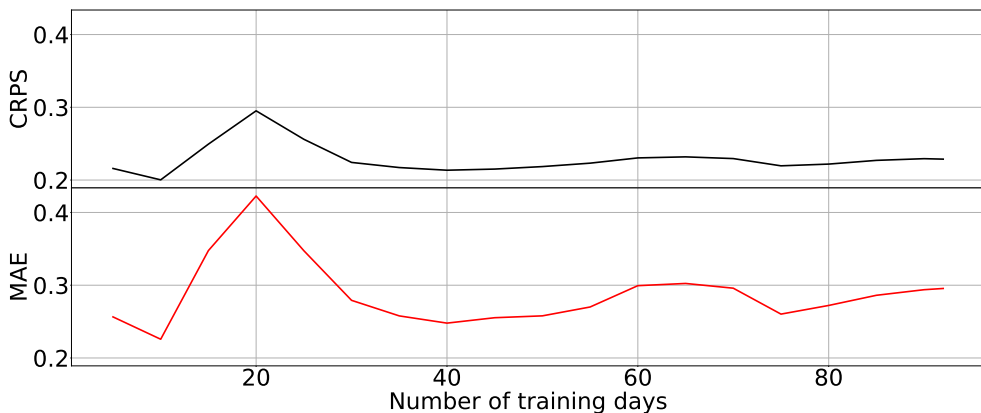


**Figure 8.** Comparison of first Wanderer mission training period lengths for  $H_s$ : MAE (top, meters), CRPS (bottom).

As can be seen from the figure 8, lowest values of MAE and CRPS are at around 10 training days. Hence, a 10 day training window was selected for Wanderer first mission. The training window selection and MAE CRPS plots for Explorer I and Wanderer II missions are presented and discussed in the supplementary material, see figure 35.

### 3.2. Ensemble forecast performance in coastal waters

In this section authors present the results of the improved forecast for the coastal areas. Explorer and Wanderer were deployed near Aran Islands, which can be considered to be in close proximity to the shore. In the next section the results of the improved forecast in the open ocean is presented.

Once the training windows are selected, the training process is performed. The algorithm works as follows, using first the Wanderer mission as an example. We take forecasts and actual recorded data from the Spotter buoy from 19 June 2020 to 29 June 2020, and predict the significant wave height for 30 June 2020. Then we move to the time period from 20 June to 30 June and predict the  $H_s$  for 1 July 2020, and keep going until the end of the Wanderer's first mission on 18 September 2020. During this process we track individual weights of each forecasting model (each broken down into three: 24H, 48H, and 72H, which results in 9 forecasts), and the overall CRPS and MAE. This process is two-fold - first we can see which individual forecasting model contributes the most to the ensemble forecast, and hence is more accurate in this instance; and we see the overall accuracy of the ensemble improved forecast. The evolution of individual weights is presented in figure 37. In similar fashion, as before, results of individual weights for Explorer I and Wanderer II are presented in the supplementary material in figure. 37.

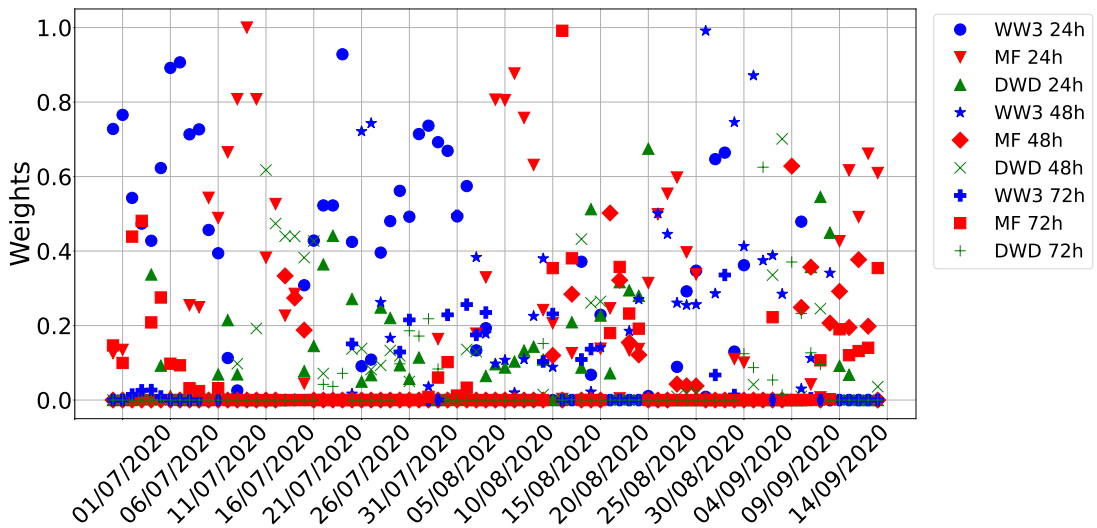


**Figure 9.** Wanderer I weights of individual forecast models. It is clearly visible, how MF is dominating the weight count towards the higher contribution to the ensemble forecast.

In addition, the authors looked at the number of effective forecasts over time. This value of entropy, shows the number of effective forecasts used in the production of the ensemble forecast. The results for Wanderer I mission is presented in figure 10. The same information for Explorer I and Wanderer II mission is presented in the supplementary material in figure 38.

One of the main reasons why the authors looked at the number of effective forecasts was to understand if the ensemble forecast is only dominated by one model at a time. From figure 10 it can be seen that there are six days where the ensemble forecast is dominated by one forecast model. However, this represents only 7.4% of the total time period. For 45.7% of the time number of effective forecasts is two, and for the 24.7% of the time, it is three. Four effective forecasts are present in the ensemble for the 14.8% of the time, and we can see that five forecasts are effective for the 7.4% of the time.

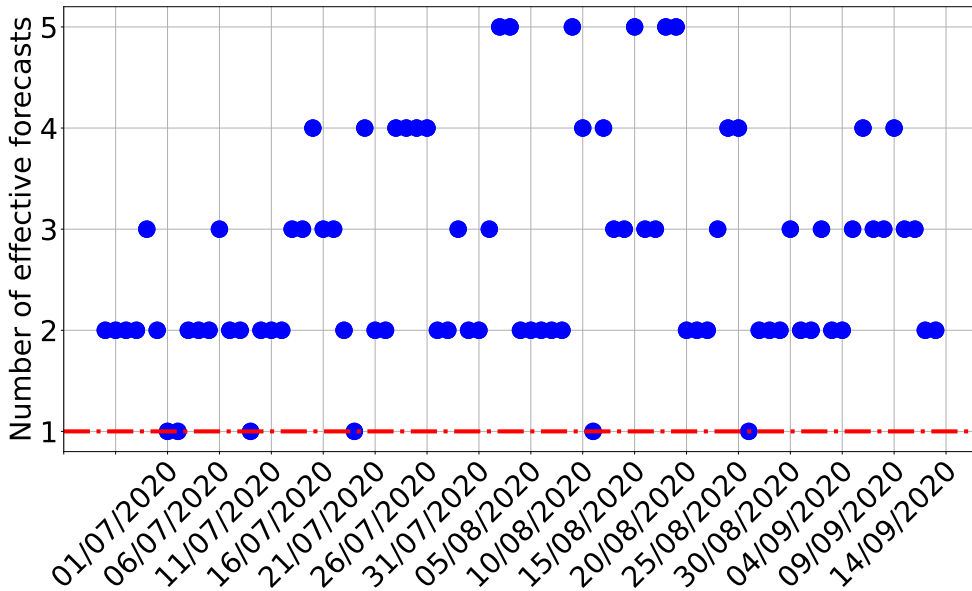


**Figure 10.** Wanderer I number of effective forecasts over time.

### 3.3. Ensemble forecast performance in the open ocean

The results mentioned in the previous section were obtained by using the historical collected forecasts and not the real time data from the Spotter buoys. A natural question arises: can the approach be extended to real-time forecasting? In this section the authors will present the results of applying the process to the real-time forecast for the M6 buoy location, off the West Coast of Ireland, for the period of 2 October 2021 to 20 October 2021. The period of the summer of 2020 was used as a training and validation example as well.

M6 is a part of the Irish Marine Weather Buoy Network. It is a joint project designed to improve weather forecasts and safety at sea around Ireland. The project is the result of collaboration between the Marine Institute, Met Eireann, The UK Met Office and the Irish Department of Transport. Data from the M6 is publicly available through the Marine Institute and Met Eireann websites, with hourly updates. M6 is located at 53.07 N,  $-15.88$  E, approximately 210 nautical miles (389 km) west southwest of Slyne Head. In addition to atmospheric variables, oceanographic data, such as  $H_s$ , wave period, maximum wave height, maximum wave period, mean direction, sea temperature, and salinity are recorded and made available to the public.

For the purpose of this exercise, the data from M6 was collected on a daily basis, and the forecasts were collected as a daily routine for the Wave Obs project. Once the forecasts were collected, training was performed, and the new HIGHWAVE forecasts for the location were produced. The actual  $H_s$  on the following date is then compared to individual forecast models and the new ensemble HIGHWAVE forecast.

As described in the previous sections, the question of the optimal training window length  $m$  was addressed before any training and ensemble forecast production was performed. To achieve this, the time period between June 2020 to September 2020 was selected. This time period is the same as the time period covered by the Explorer first mission and Wandered first mission. Looking at straight forward forecast versus M6 measurements, we see a good agreement between the two, with the expected behaviour of 24H forecast being more accurate than 48H or 72H (see figures 11 (summer/autumn), and 12 (winter), and the values of MAE and MAPE in table 2).

Table 4 presents the mean absolute percentage error of individual forecasting models for the original forecasts (left columns) and bias corrected forecasts (right columns). The MAPE of the HIGHWAVE forecast was equal to 0.12. Comparing this value to the individual models, note the reduction in error can be as significant as 48%. And the forecast improvement can be as high as 8%.

We would like to point out two observations one can make from this comparison. First - the values of MAE are lower for this location, compared to MAE values for the forecast near the Aran Islands. This is a direct confirmation that the forecast models considered are much better at predicting sea state in the open ocean (recall the M6 location). However, forecast accuracy starts to decrease as we get closer to the shore.

Selection of the sliding training window is based on the values of CRPS and MAE, as it was previously for the Spotter buoy missions. The training for a specific date was performed using 5, 10, 15, 20, to 85 training days at a time, for two different periods - summer and winter (figure 13). It appears that 20 training days is a reasonable training period. From figure 13 one can notice that 50 days seem even better – however, the authors opted for a shorter training period, due to the reasons mentioned before. One can notice the increase in the error in the winter period, similar to the Explorer I mission. This will be addressed further in the publication.

Before live training and production of the ensemble forecast began, the suggested approach was tested on the aforementioned summer and winter periods. Using a range of training windows between 5 and 95 days the overall values of MAE and CRPS were calculated for the ensemble forecasts, see figure 13. In the summer period both MAE and CRPS decrease with increasing training day period, as it was seen before in the Wanderer I mission. The winter period, however, displays a behaviour where the error is increasing with increasing training window, this will be discussed separately. Looking at individual forecast model weights contributing most to the ensemble forecast, one can note that the

**Table 2.** Mean absolute error (winter, m) and mean absolute percentage error (summer, %) of individual raw forecasting models, depending on the forecast time for M6

Mission	24H				48H				72H			
	DWD	WW3	MF	MI	DWD	WW3	MF	MI	DWD	WW3	MF	MI
M6 Summer	0.20	0.14	0.10	–	0.13	0.15	0.12	–	0.18	0.19	0.15	–
M6 Winter	0.33	0.39	0.33	0.33	0.60	0.46	0.43	0.42	0.49	0.39	0.45	0.39
HIGHWAVE (winter)	0.31				0.31				0.31			

**Table 3.** Mean absolute error (winter, m) and mean absolute percentage error (summer, %) of individual adjusted forecasting models, depending on the forecast time for M6

Mission	24H				48H				72H			
	DWD	WW3	MF	MI	DWD	WW3	MF	MI	DWD	WW3	MF	MI
M6 Summer	0.21	0.12	0.11	–	0.14	0.14	0.13	–	0.19	0.19	0.16	–
M6 Winter	0.44	0.40	0.31	0.32	0.58	0.47	0.42	0.44	0.56	0.47	0.45	0.49

**Table 4.** Mean absolute percentage error of individual forecasting models, depending on the forecast time for M6 summer period (%).

Model	24H		48H		72H	
	Original Forecast	Adjusted Forecast	Original Forecast	Adjusted Forecast	Original Forecast	Adjusted Forecast
DWD	0.2	0.21	0.13	0.14	0.18	0.19
MF	0.10	0.11	0.12	0.13	0.15	0.16
WW3	0.14	0.12	0.15	0.14	0.19	0.19



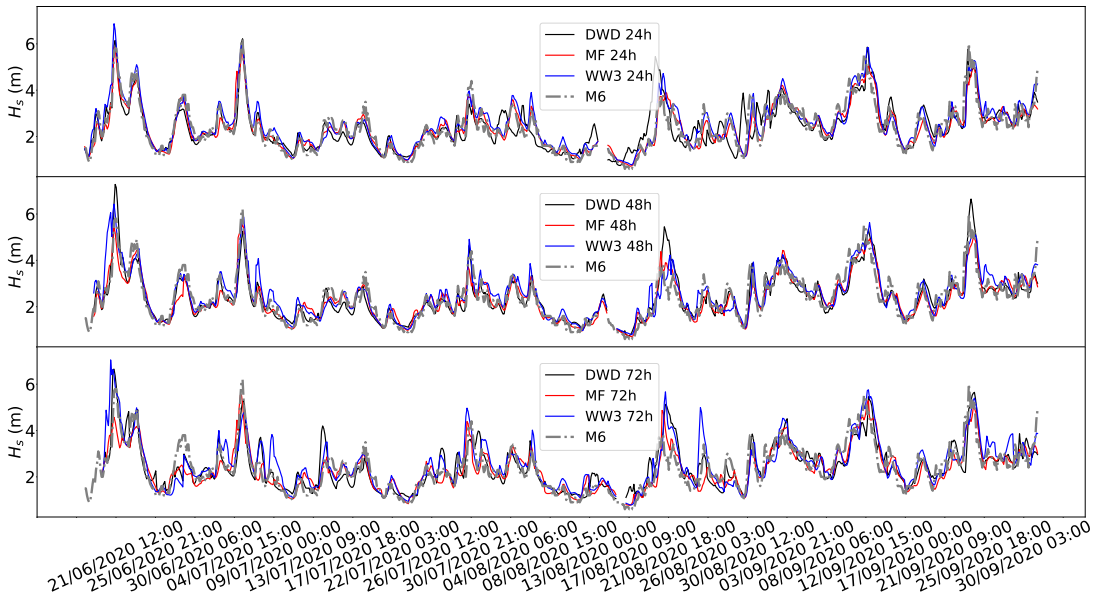


**Figure 11.** M6 Met buoy area forecast from WW3, MF and DWD for 24h (top), 48h (middle), and 72h (bottom).

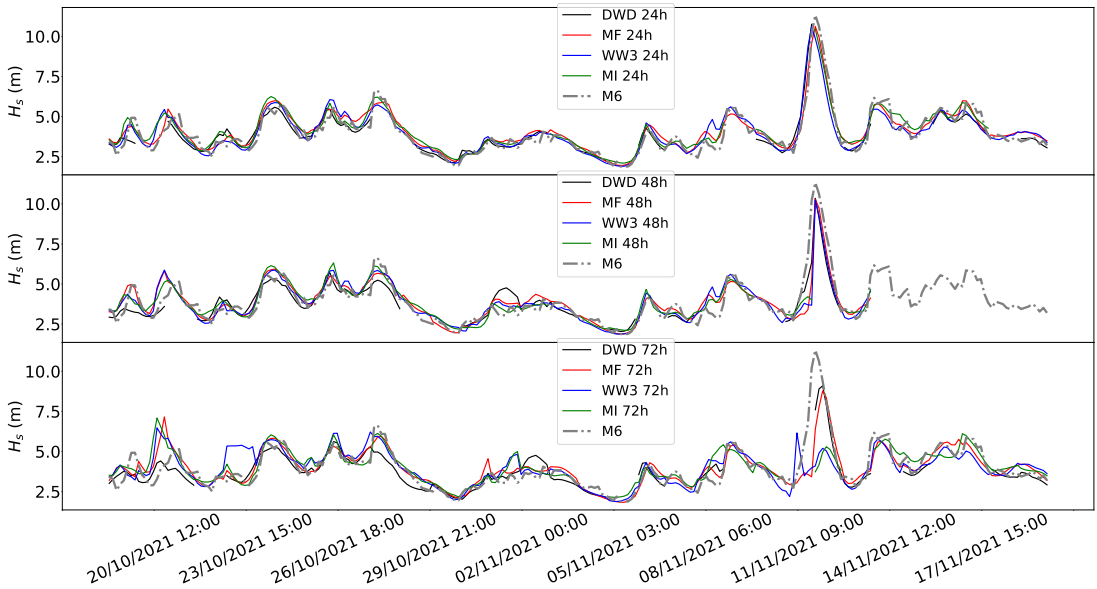


**Figure 12.** M6 Met buoy area forecast from WW3, MF, MI, and DWD for 24h (top), 48h (middle), and 72h (bottom), for the winter period.

MF and WW3 forecasts had dominant weights across the two periods, see figure 14. We will address the question of weights of the individual models later. It is obvious that the ensemble forecast is more accurate than the raw un-adjusted individual forecast models. However, an additional question was asked: would individual bias-corrected model would perform better than the ensemble forecast? As discussed in the Statistics section, as part of the ensembleBMA software, correction coefficients for

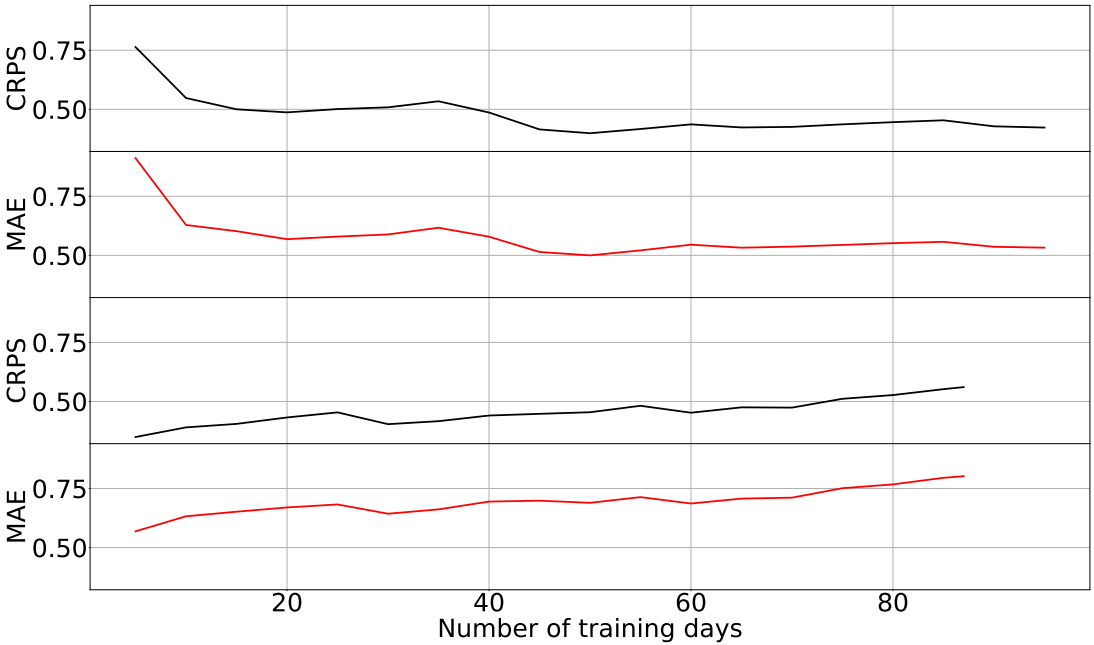


**Figure 13.** Selection of the training window for the M6 ensemble forecast during the summer period (top) and the winter period (bottom). MAE in meters..

each individual model can be obtained. In the next section we present individual adjusted forecasts compared to the ensemble forecast. Values for the MAE and MAPE are presented in tables 2 for the raw and 3 adjusted forecasts.

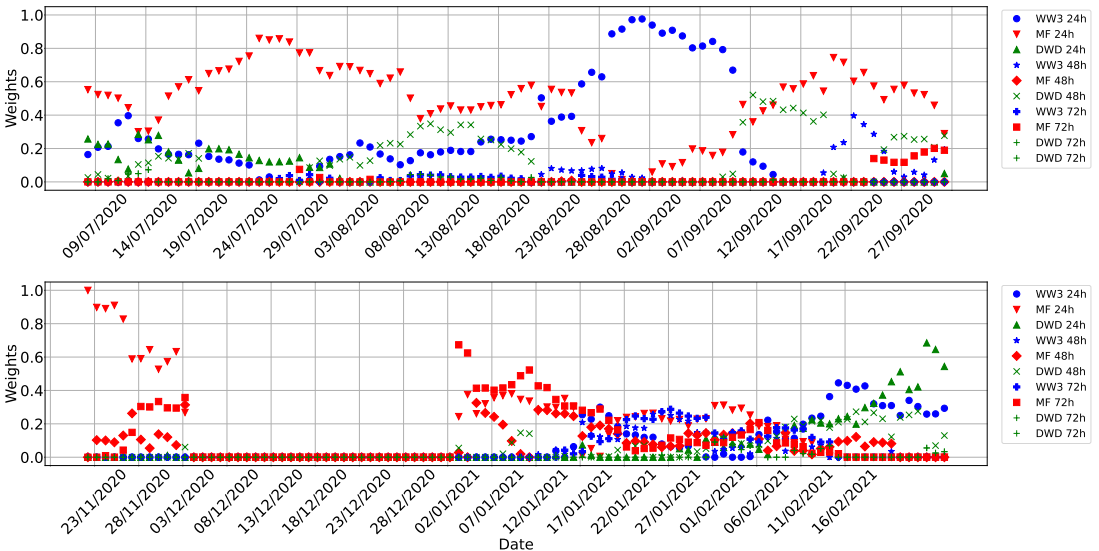


**Figure 14.** Weights of individual un-adjusted forecast models for the summer period (top) of 2020 and winter (bottom), at M6 buoy location.

Similar to the Wanderer I, the authors looked at the effective number of forecasts for the both periods at the M6 buoy. The results are presented in figure 15.

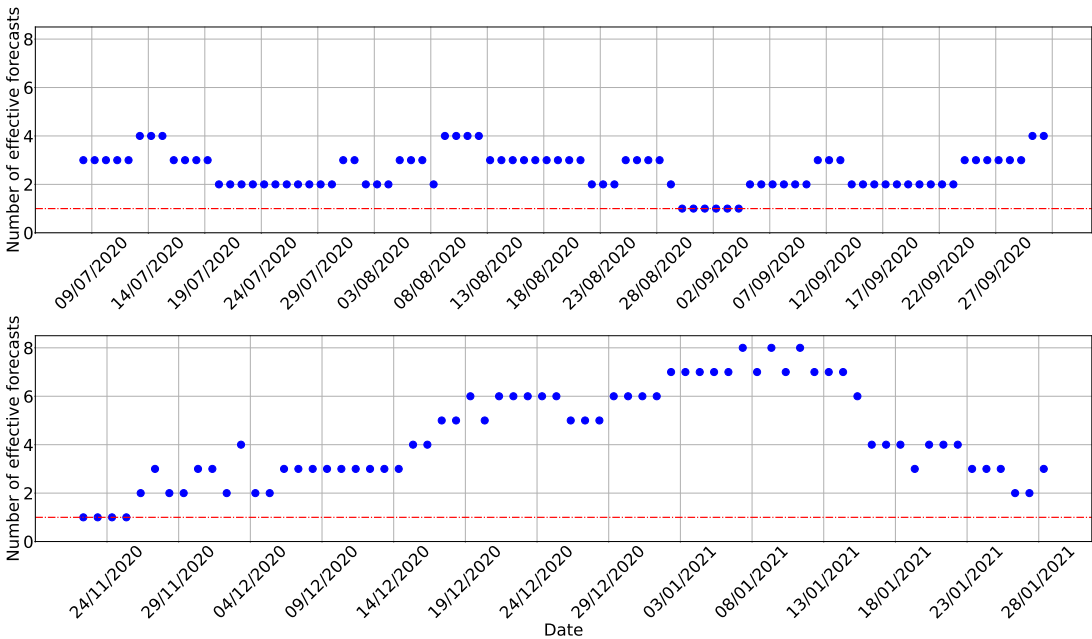


Figure 15. Number of effective forecasts for M6 summer (top) and winter (bottom) period.

3.3.1. Individual bias-corrected forecast performance versus the ensemble forecast

In this subsection authors compare the performance of the combined ensemble forecast (denoted HIGHWAVE) to individual bias-corrected models. As described above, this was 'live' daily training between 2 October 2021 and 20 October 2021. It was performed with free ensembleBMA software and publicly available forecasts from each model mentioned here and below. The training was performed on a Intel(R) Core(TM) i7-4710HQ CPU @ 2.50GHz 2.49 GHz processor, with 16.0 GB RAM, and took seconds. There was no additional time spent on the forecast data collection, as it is a part of the automated process of Wave Obs.

In figures 17 and 18 one can see that the adjusted MAPE or MAE in the case of winter period is lower on particular days, than the MAPE or MAE of the ensemble forecast. However, overall, over the whole period, HIGHWAVE ensemble forecast is on average more accurate than any raw or adjusted individual models.

On average, over a month, taking into consideration all four models, the ensemble forecast produced, using the BMA techniques is at least  $\approx 1\%$  better than individual forecasting models, and  $3\%$  better on average. On a few days individual forecast models performed better than the ensemble forecast. However, this number is negligible, and this is reflected in the overall MAE values. The visual comparison of the HIGHWAVE ensemble forecast to the M6 buoy observation is presented in figure 19.

In addition, from this set of data, it is clear that MF (24H) has the highest weight  $45\%$  of the time, followed by WW3 (24H)  $28\%$ , and DWD (24H)  $10\%$  of the time. Figure 20 visualizes the contribution of each individual model in the ensemble forecast for the summer period.

For the winter period, it is surprising to see that the 72H forecast has the dominant effect on the contribution towards the ensemble forecast.

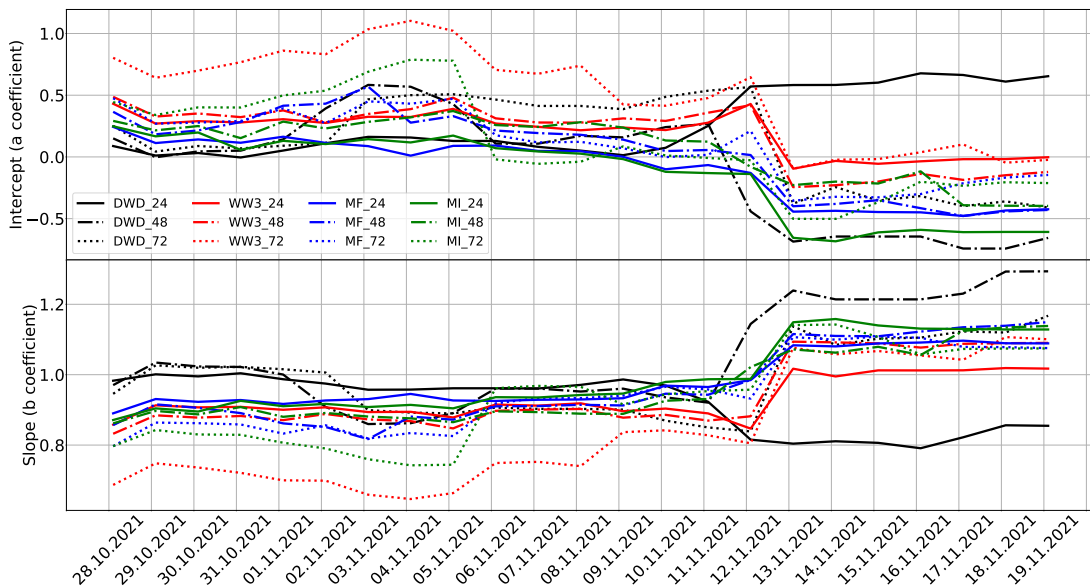


**Figure 16.** Bias coefficients for the corrected forecasts: intercept (a) - top panel, slope (b) - bottom panel.

There is no particular pattern, as the forecast having the highest impact does change. There would be a week or two where for example one is dominating. For example, from 30 June 2020 till 07 July 2020, DWD 24 H forecast has the highest weight. But then it can change to MF taking over for a week. The reasons behind that could be an extension to the present work.

#### 4. Discussion and concluding remarks

The results of the present study indicate that it is possible to produce an averaged forecast for a particular location, with the accuracy at least  $\approx 1\%$  higher than any available model discussed in this work. The accuracy can be further improved upon by selecting a suitable training window, and possibly adjusting the weights of individual models, depending on the time of year, as we saw that different models perform better under different conditions. The 1% improvement might not seem like a lot at first sight. However, this is still an improvement, and it should be noted that it is 'at least 1%'. In reality, we are looking at improvement of the forecast up to 8%. If we were to look at the reduction of error, in M6 case presented in the paper, we see the range of the mean absolute percentage error reduction between 1 – 9%, see table 4, with HIGHWAVE forecast yielding a 0.12 value for the MAPE. In the case of forecast improvement for the M6 winter period, we see the error reduction between the minimum of 6% to substantial 48%. This is comparable with other attempts at wave forecast improvement, see for example [Callens A., Morichon D., Abadie S., Delpy M., Liquet B., 2020], where random forest and gradient boosting trees were used to improve wave forecast at a specific location, and the authors achieve a 39.8% error decrease in their proposed method, which is comparable with our range of 6 – 48%. Other attempts, mostly involving Machine Learning and Neural Networks have been a highlight in recent years, see for example [Londhe S.N., Shah S., Dixit P.R., Balakrishnan Nair T.M., Sirisha P., Jain R., 2016] for a coupled numerical and artificial neural network model for improving location specific wave forecast. In similar fashion the tidal predictions were addressed, see for example [Yin J-C., Zou Z-J., Xu F., 2013].

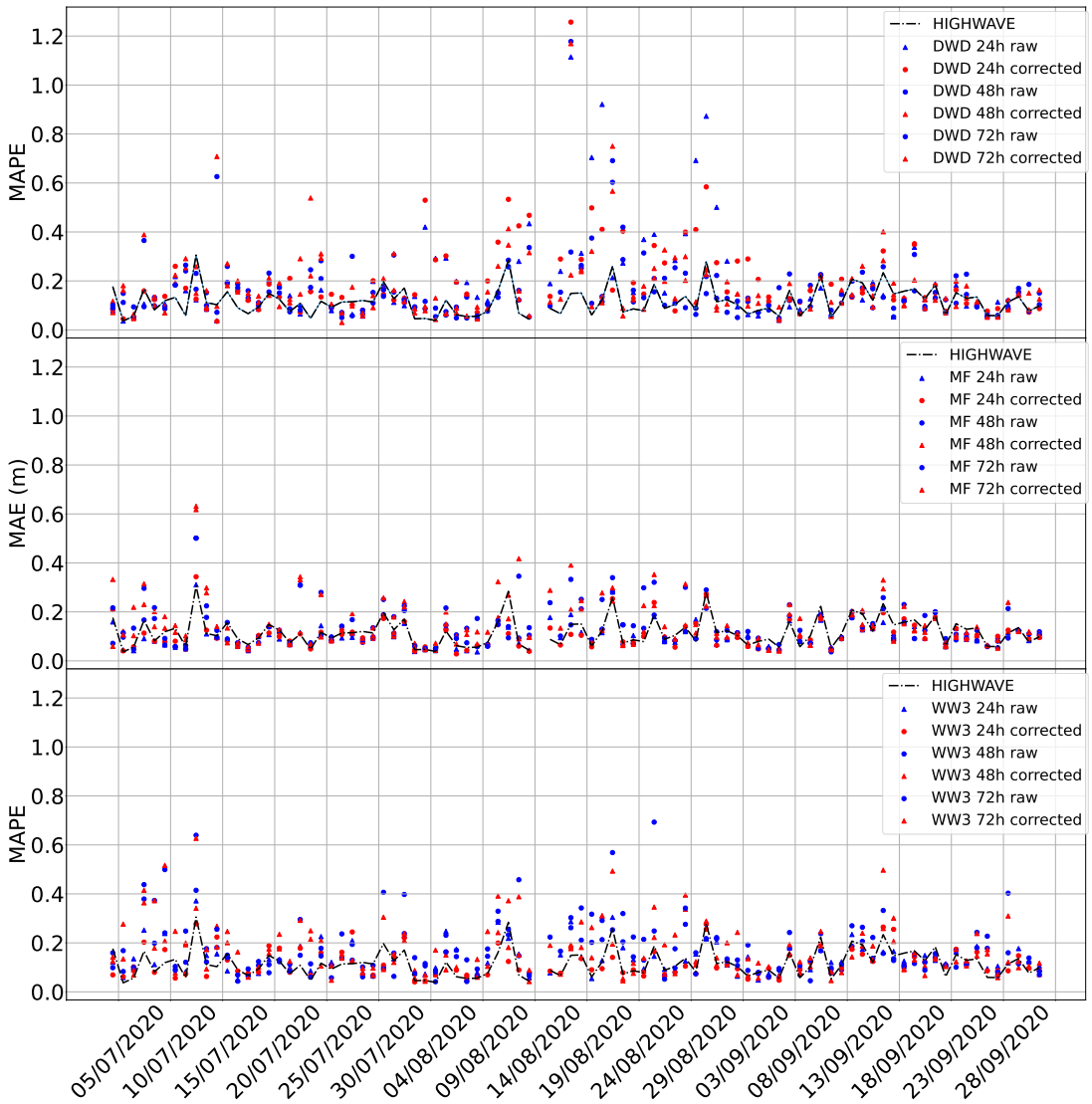


**Figure 17.** Daily MAPE (%) of individual DWD – raw, – adjusted, and HIGHWAVE (top panel); MF – raw, – adjusted, and HIGHWAVE (middle panel); WW3 – raw, – adjusted, and HIGHWAVE (bottom panel) forecasts for the summer period in the M6 location.

We believe that it is a good improvement, since the shores on the West Coast of Ireland experience waves reaching very steep values during winter storms (O’Brien L., Dudley J. M., Dias F. [2013], O’Brien L., Renzi E., Dudley J. M., Clancy C., Dias F. [2018]). It is not computationally expensive, and can be completed without the use of cluster or any type of high performance computing. Implementing the forecast collection process is straightforward. It only requires the Wave Obs package, available on GitHub. EnsembleBMA software used for training of the forecasts is free software available from cran.r-project.org. This free access to information and the straight forward process of collecting and training the forecast opens up the opportunity to wider population to use this tool for their daily needs. This might appeal to harbour-masters, fisherman, and others who depend on the accurate sea state forecast. Of course, the authors are aware of recent works in the forecast improvement area with Machine

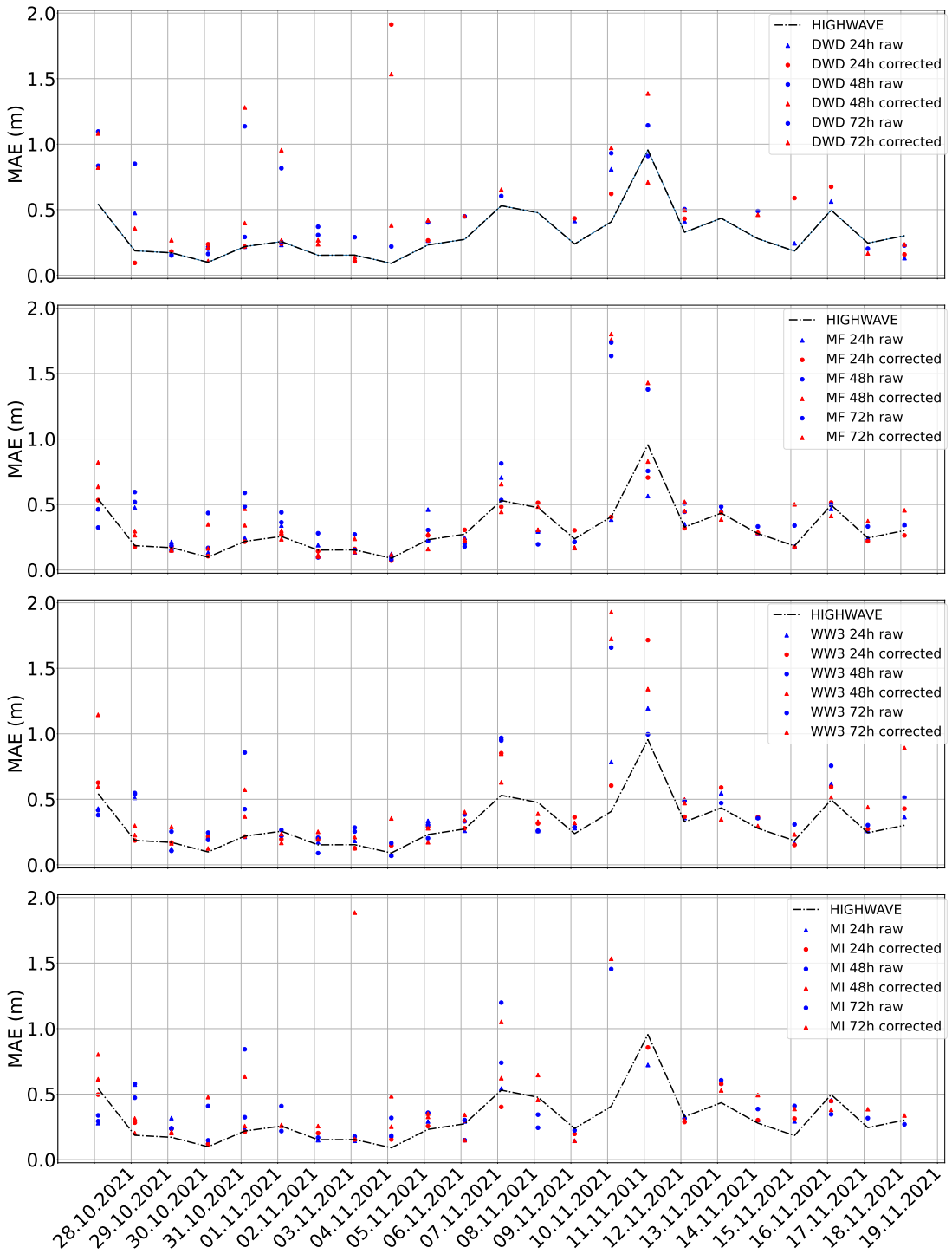


**Figure 18.** Daily MAE of individual DWD – raw, - adjusted, and HIGHWAVE (top panel); MF – raw, – adjusted, and HIGHWAVE (second panel); WW3 – raw, – adjusted, and HIGHWAVE (third panel); MI – raw, – adjusted forecasts for the winter period in the M6 location.

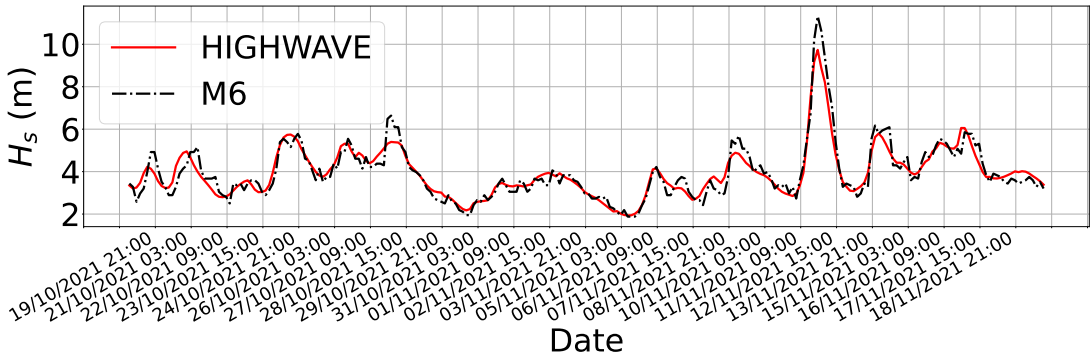


**Figure 19.** Ensemble forecasts (HIGHWAVE) produced by the procedure proposed in this publication compared to the actual record from the M6 buoy for the winter period.

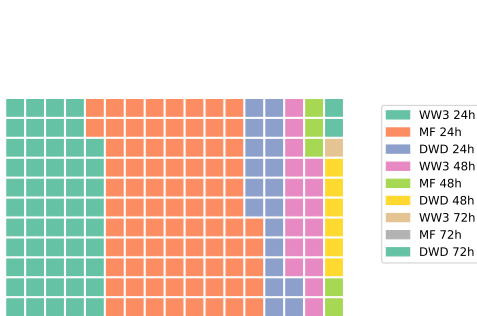


**Figure 20.** Visual representation of each individual model having the highest weight on the ensemble forecasts for the period of interest.



**Figure 21.** Visual representation of each individual model having the highest weight on the ensemble forecasts for the winter period.

Learning algorithms (Guillou N., Chapalain G. [2021], Gracia S., Olivito J., Resano J., Martin-del-Brio B., de Alfonso M., Álvarez E. [2021], amongst many others). Readers interested in Machine Learning algorithms are referred to Ali A., Fathall A., Salah A., Bekhit M., Eldesouky E. [2021] for evaluation of Machine Learning, Deep Learning, and Statistical Predictive Models. However, the nature of ML requires specific knowledge and training to perform such improvements. For example in Wu M., Stefanakos C., Gao Z. [2020], PBML model has MAE of 0.1961 for 24 h lead time forecast of the  $H_s$ , to be compared with the HIGHWAVE MAE of  $\approx 0.08$  for the 24 h forecast. In no way the authors are trying to downshift the role of ML algorithms in improving the sea state forecasting. However, one can consider different applications of ML and Wave Obs. Where ML can be used on a large scale predictions, it might be beneficial, on a local scale, in terms of how easy it is to use, and the low computational cost of the Wave Obs process to be considered as a possibility for a non-scientific community audience.

The only issue is the availability of real-time or even historical data for the purposes of training. If there are some buoys in the area of interest and the data is publicly available - one can produce improved ensemble forecasts using the combination of the recorded measurements and available forecasts. However, if there is no field data available, the training process would suffer from the lack of data.

We investigated the possibility of extending this improved forecast to all coastal areas around Ireland. It was found that there exist 11 buoys that have the live data available to the public that can be used in the training process. However, the distribution of the buoys would not allow for cross-coverage

of the whole coastal area, please refer to figure 22 to see the locations, and the extent of the forecast resolution around each buoy.

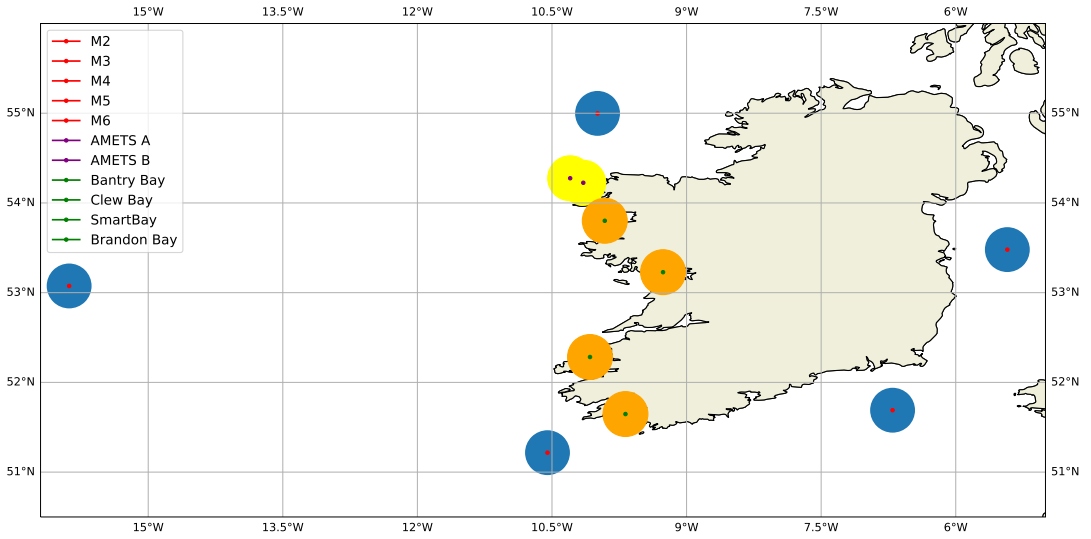


**Figure 22.** Map of buoys with open-access data around Ireland.

Despite the issues in extending the improved ensemble forecast to global scale, it can be concluded if a particular area requires a more accurate forecasting (due to fishing, sailing, or transportation activities) it can easily be achieved using the approach described in this publication.



**Abbreviations.** API Application Programming Interface  
 BMA Bayesian Model Averaging  
 CPU Central Processing Unit  
 CRPS Continuous Rank Probability Score  
 CDF Cumulative Distribution Function  
 DWD Deutscher Wetterdienst (German weather forecasting service)  
 ERDDAP Environmental Research Division's Data Access Program  
 ERC European Research Council  
 FNMOC Fleet Numerical Meteorology and Oceanography Center  
 GFS Global Forecast System  
 ICON Icosahedral Nonhydrostatic Model  
 JSON JavaScript Object Notation  
 ML Machine Learning  
 MI Marine Institute  
 MAE Mean Absolute Error  
 MAPE Mean Absolute Percentage Error  
 MF Météo-France  
 MRS Mobile Research Station  
 NCEP National Centers for Environmental Prediction  
 NOAA National Oceanic and Atmospheric Administration  
 RAM Random-access memory  
 SHOM Service Hydrographique et Océanographique de la Marine  
 SWAN Simulating Waves Nearshore  
 WAM the Wave Model  
 THREDDS Thematic Real-time Environmental Distributed Data Services  
 UW University of Washington  
 WW3 Wavewatch III

**Acknowledgments.** We acknowledge Arnaud Disant for the idea of the alert service, the Wave Group members who contributed to daily collection and publishing of the forecasts, the Aran Island community for providing eye witness evidence of some events, and the reviewers for their valuable and thoughtful comments and efforts towards improving our manuscript.

**Funding Statement.** This work was supported by the European Research Council (ERC) under the research project ERC-2018-AdG 833125 HIGHWAVE; Science Foundation Ireland (SFI) under Grant number SFI/12/RC/2289\_P2; and Science Foundation Ireland (SFI) under Marine Renewable Energy Ireland (MaREI), the SFI Centre for Marine Renewable Energy Research (grant 12/RC/2302).

**Competing Interests.** Competing interests: The authors declare none.

**Data Availability Statement.** Wave Obs toolkit is not publicly accessible at present, but the authors will share it upon request through GitHub repository. [ensembleBMA software is available through ensembleBMA](#). Forecast data has been obtained from PlanetOS API, Met Éireann data interface, and the ERDDAP servers of NOAA/NCEPCoastWatch, Pacific Islands Ocean Observing System (PacIOOS) and Irish Marine Institute. Likewise, M6 data can be freely obtained from Marine Institute website. Historical forecasts for the Aran Island area are available upon request at [HIGHWAVE](#).

**Ethical Standards.** The research meets all ethical guidelines, including adherence to the legal requirements of the study country.

**Author Contributions.** Conceptualization: B.M.; F.D. Methodology: B.M; T.K.; D.S. Data curation: F.D. Data visualisation: T.K. Writing original draft: T.K; D.S.; F.D.; B.M. All authors approved the final submitted draft.

## References

- Ali A., Fathall A., Salah A., Bekhit M., Eldesouky E. Marine data prediction: an evaluation of machine learning, deep learning, and statistical predictive models. *Computational Intelligence and Neuroscience*, 2021:13, 2021. doi: 10.1155/2021/8551167.
- Babanin A. *Breaking and dissipation of ocean surface waves*. Cambridge University Press, 2011. doi: 10.1017/CBO9780511736162.
- Barthelemy X., Banner M. L., Peirson W. L., Fedele F., Allis M., Dias F. On a unified breaking onset threshold for gravity waves in deep and intermediate depth water. *Journal of Fluid Mechanics*, 841:463 – 488, 2018. doi: 10.1017/jfm.2018.93.
- Brier G. W., Allen R. A. Verification of weather forecasts. *Compendium of meteorology: prepared under the direction of the committee on the compendium of meteorology*, pages 841–848, 1951. doi: 10.1007/978-1-940033-70-9\_68.
- Callens A., Morichon D., Abadie S., Delpy M., Liquet B. Using random forest and gradient boosting trees to improve wave forecast at a specific location. *Applied Ocean Research*, 104:102339, 2020. doi: <https://doi.org/10.1016/j.apor.2020.102339>.
- Dempster A. P., Laird N. M., Rubin D. B. Maximum likelihood from incomplete data via the EM algorithm. *Journal of the Royal Statistical Society. Series B. Methodological*, 39(1):1 – 38, 1977. doi: 10.2307/2984875.
- Derakhti M., Banner M. L., Kirby J. T. Predicting the breaking strength of gravity water waves in deep and intermediate depth. *Journal of Fluid Mechanics*, 848:R2, 2018. doi: 10.1017/jfm.2018.352.
- Ducrozet G., Gouin M. Influence of varying bathymetry in rogue wave occurrence within unidirectional and directional sea-states. *Journal of Ocean Engineering and Marine Energy*, 3:309 – 324, 2017. doi: 10.1007/s40722-017-0086-6.
- Fraleigh C., Raftery A. E., Gneiting T., Sloughter J. M. EnsembleBMA: an R package for probabilistic forecasting using ensembles and Bayesian model averaging. Technical Report 516R, Department of Statistics, University of Washington, 2008.
- Fuentes M., Raftery A. E. Model evaluation and spatial interpolation by Bayesian combination of observations with outputs from numerical models. *Biometrics*, 61(1):36–45, 2005. doi: 10.1111/j.0006-341X.2005.030821.x.
- Gallagher S., Gleeson E., Tiron R., McGrath R., Dias F. Wave climate projections for Ireland for the end of the 21st century including analysis of EC-Earth winds over the North Atlantic Ocean. *International Journal of Climatology*, 36(14):4592–4607, 2016. doi: <https://doi.org/10.1002/joc.4656>.
- Gallagher S., Tiron R., Dias F. A long-term nearshore wave hindcast for Ireland: Atlantic and Irish Sea coasts (1979–2012). *Ocean Dynamics*, 64:1163–1180, 2014. doi: 10.1007/s10236-014-0728-3.
- Gneiting T., Raftery A. E. Strictly proper scoring rules, prediction, and estimation. *Journal of the American Statistical Association*, 102(477):359 – 378, 2007. doi: 10.1198/016214506000001437.
- Gneiting T., Raftery A. E. Weather forecasting with ensemble methods. *Science*, 310(5746):248 – 249, 2015. doi: 10.1126/science.11152.
- Gneiting T., Raftery A. E., Westveld A. H., Goldman T. Calibrated probabilistic forecasting using ensemble model output statistics and minimum CRPS estimation. *Monthly Weather Review*, 133(5):1098 – 1118, 2005. doi: 10.1175/MWR2904.1.
- Gracia S., Olivito J., Resano J., Martin-del-Brio B., de Alfonso M., Álvarez E. Improving accuracy on wave height estimation through machine learning techniques. *Ocean Engineering*, 236:108699, 2021. doi: 10.1016/j.oceaneng.2021.108699.
- Grimmett E. P., Mass C. F. Initial results of a mesoscale short-range ensemble forecasting system over the pacific northwest. *Weather and Forecasting*, 17(2):192 – 205, 2002. doi: 10.1175/1520-0434(2002)017<0192:IROAMS>2.0.CO;2.
- Guillou N., Chapalain G. Machine learning methods applied to sea level predictions in the upper part of a tidal estuary. *Oceanologia*, 63(4):531 – 544, 2021. doi: 10.1016/j.oceano.2021.07.003.
- Hoeting J. A., Madigan D., Raftery A. E., Volinsky C. T. Bayesian model averaging: a tutorial. *Statistical Science*, 14(4):382 – 417, 1999. doi: 10.1214/ss/1009212519.
- Kass R. E., Raftery A. E. Bayes factors. *Journal of the American Statistical Association*, 90(430):773 – 795, 1995. doi: 10.2307/2291091.
- Kuik A. J., van Vledder G. Ph., Holthuijsen L. H. A method for the routine analysis of pitch-and-roll buoy wave data. *Journal of Physical Oceanography*, 18(7):1020 – 1034, 1988. doi: 10.1175/1520-0485(1988)018<1020:AMFTRA>2.0.CO;2.
- Leamer E. E. *Specification searches*. Wiley, 1978.
- Londhe S.N., Shah S., Dixit P.R., Balakrishnan Nair T.M., Sirisha P., Jain R. A coupled numerical and artificial neural network model for improving location specific wave forecast. *Applied Ocean Research*, 59:483–491, 2016. doi: <https://doi.org/10.1016/j.apor.2016.07.004>.
- Monirul Qader Mirza M. Climate change and extreme weather events: can developing countries adapt? *Climate Policy*, 3(3): 233 – 248, 2003. doi: 10.1016/S1469-3062(03)00052-4.
- O'Brien L., Dudley J. M., Dias F. Extreme wave events in Ireland: 14 680 BP–2012. *Natural Hazards and Earth System Sciences*, 13(3):625 – 648, 2013. doi: 10.5194/nhess-13-625-2013.
- O'Brien L., Renzi E., Dudley J. M., Clancy C., Dias F. Catalogue of extreme wave events in Ireland: revised and updated for 14680 BP to 2017. *Natural Hazards and Earth System Sciences*, 18(3):729 – 758, 2018. doi: 10.5194/nhess-18-729-2018.
- Raftery A. E., Gneiting T., Balabdaoui F., Polakowski M. Using Bayesian model averaging to calibrate forecast ensembles. *Monthly Weather Review*, 133(5):1155 – 1174, 2005. doi: 10.1175/MWR2906.1.
- Raghukumar K., Chang G., Spada F., Jones C., Janssen T., Gans A. Performance characteristics of “Spotter,” a newly developed real-time wave measurement buoy. *Journal of Atmospheric and Oceanic Technology*, 36(6):1127 – 1141, 2019. doi: 10.1175/JTECH-D-18-0151.1.

- Sloughter J. M., Gneiting T., Raftery A. E.** Probabilistic wind vector forecasting using ensembles and Bayesian model averaging. *Monthly Weather Review*, 141(6):2107 – 2119, 2013. doi: 10.1175/MWR-D-12-00002.1.
- Sloughter J.M., Raftery A.E., Gneiting T., Fraley C.** Probabilistic quantitative precipitation forecasting using bayesian model averaging. *Monthly Weather Review*, 135:3209 – 3220, 2007. doi: <https://doi.org/10.1175/MWR3441.1>.
- Sofar Ocean Technologies.** User guide, 2022. URL [https://assets.website-files.com/6195779003438046f0c9adde/62d824173567b6550fb23072\\_Spotter\\_User\\_Guide.pdf](https://assets.website-files.com/6195779003438046f0c9adde/62d824173567b6550fb23072_Spotter_User_Guide.pdf).
- The Wamdi Group.** The WAM model — a third generation ocean wave prediction model. *Journal of Physical Oceanography*, 18(12):1775 – 1810, 1988. doi: 10.1175/1520-0485(1988)018<1775:TWMTGO>2.0.CO;2.
- Tian Z., Perlin M. G., Choi W.** Energy dissipation in two-dimensional unsteady plunging breakers and an eddy viscosity model. *Journal of Fluid Mechanics*, 655:217 – 257, 2010. doi: 10.1017/S0022112010000832.
- Tian Z., Perlin M. G., Choi W.** An eddy viscosity model for two-dimensional breaking waves and its validation with laboratory experiments. *Physics of Fluids*, 24(3):036601, 2012. doi: 10.1063/1.3687508.
- United Nations.** Factsheet: people and oceans. URL <https://www.un.org/sustainabledevelopment/wp-content/uploads/2017/05/Ocean-fact-sheet-package.pdf>.
- Wu M., Stefanakos C., Gao Z.** Multi-step-ahead forecasting of wave conditions based on a physics-based machine learning (PBML) model for marine operations. *Journal of Marine Science and Engineering*, 8(12), 2020. doi: 10.3390/jmse8120992.
- Yin J-C., Zou Z-J., Xu F.** Sequential learning radial basis function network for real-time tidal level predictions. *Ocean Engineering*, 57:49–55, 2013. ISSN 0029-8018. doi: <https://doi.org/10.1016/j.oceaneng.2012.08.012>.

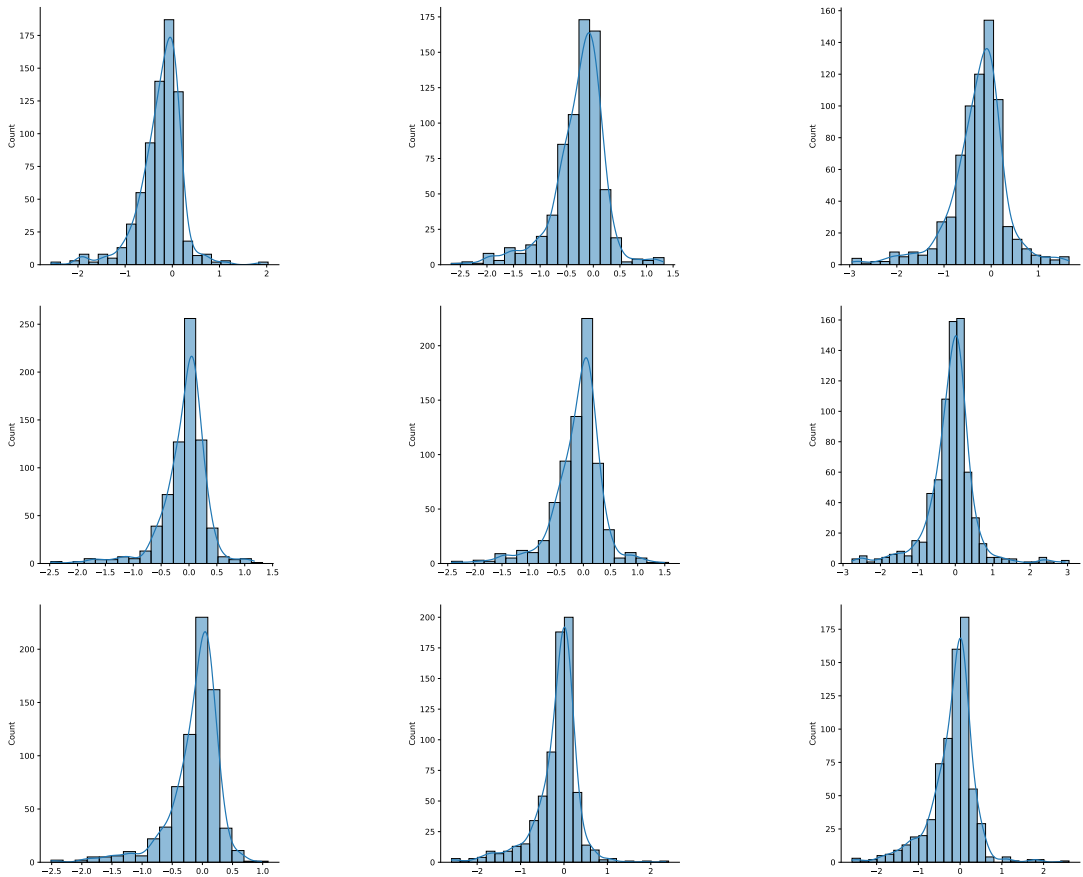


**Figure 23.** Histograms of the difference between the original forecast for Wanderer I mission versus the actual observed value. From top to bottom: DWD, WW3, MF; from left to right: 24H, 48H, 72H.

**Supplementary Material.** Authors provide the following supplementary material with the publication. The plots provided below are complimentary to the plots presented in the main body of the publication.

### ***S1 Forecasts versus buoy observations***

In the main body of the article, we investigated the normality assumption by comparing the observed significant wave height to the bias-adjusted forecasts using histograms and QQ-plots, and presenting the results for the adjusted M6 winter period. Below we present all other missions - Explorer I, Wanderer I, Wanderer II, M6 summer, and M6 winter unadjusted.

In the main body of the article, authors present the comparison between the  $H_s$  recorded by the Wanderer buoy and the three model forecasts for the period between 15 June 2020 and 15 September 2022. In the same section 3, Results, authors make a reference to results for the second Wanderer and first Explorer missions. And the MAE for these two additional missions is presented in table 1. Actual 'brute force' comparison with the Wanderer and Explorer data and model forecasts is plotted in figures 33 and 34.

During Explorer's first mission, it went adrift on 5 September 2020. In the results presented, authors only concentrate on the period where the buoy stayed anchored in one geographical spot. But it is still beneficial to look at the drifting period.

While adrift, Explorer was approaching the shoreline. Closer to the shore the water depth is decreasing, and we see that the values of the  $H_s$  are lower than the predicted values. In general, it is expected to see larger waves closer to shore. This is well explained by the wave behaviour when waves transition from deep water to shallow water. This can be understood by looking at wave speeds. Once in deep water, the wave speed depends on the wavelength. However, once the waves enter shallow water, the wave behaviour is affected by the bathymetry. As waves feel the bottom, they slow down, and following waves 'catch up' with waves in front, so the wavelength is decreased. In this process, the energy contained in the wave is constant, hence the wave grows, and one is supposed to see higher waves. However, waves cannot grow infinitely: once a certain threshold is reached

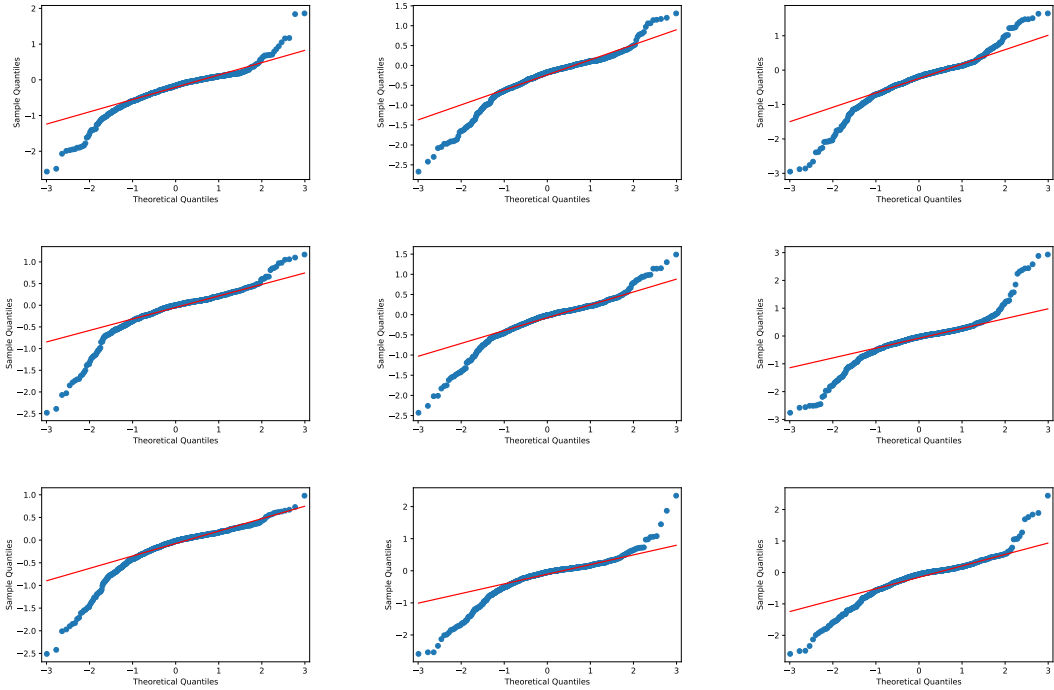


**Figure 24.** *Q-Q plots of the difference between the original forecast for Wanderer I mission versus the actual observed value. From top to bottom: DWD, WW3, MF; from left to right: 24H, 48H, 72H.*

waves break (see for example Tian Z., Perlin M. G., Choi W. [2010], Tian Z., Perlin M. G., Choi W. [2012], Ducrozet G., Gouin M. [2017], Derakhti M., Banner M. L., Kirby J. T. [2018], Barthelemy X., Banner M. L., Peirson W. L., Fedele F., Allis M., Dias F. [2018], and the book by Babanin A. [2011]). Here we leave the process of breaking aside, but it is important to understand that shoaling waves grow and can eventually break. This is exactly what we see in figure 33, after the vertical black line that denotes drifting. The observed value of  $H_s$  is lower than the one predicted for the area with larger depth, but the shape of the evolution of the observed  $H_s$  compares very well to the shape of the forecast.

**S2 Training window selection for the Wanderer II and Explorer I missions**

In section 3. Results, authors discuss the selection of the sliding training window for the ensemble forecasts. The Wanderer I mission is used as an example, and the plots are presented in the main body of the article. Here the authors present similar plots, but for the Explorer I and Wanderer II missions. As previously discussed, longer training period is not always necessary. In the Wanderer II case, we see a plateau after certain number of training days is reached. Both MAE and CRPS for Wanderer II mission are presented in figure 35 top panels.

We see a different picture for Explorer, see figure 35 (bottom panels) - we see how both the MAE and CRPS are increasing with the number of training days, hence the shortest training period was selected for Explorer. To understand this error increasing behaviour in Explorer’s training, we looked separately at training 24, 48, and 72 hour forecasts, the information regarding these separate training periods is presented in figure 36.

The 24H forecast displays the expected behaviour: decreasing values of MAE and CRPS with an increasing number of training days, with a plateau at some point. However, 48H and 72H forecasts appear to increase in MAE and CRPS values. The authors do not have a concrete explanation for this behaviour of 48H and 72H forecasts. However, one of the possible explanations is that as we know that 48H and 72H carry more inaccuracies than 24H ones, and with increasing training window, we keep accumulating the errors, thus increasing the values for MAE and CRPS. Accordingly, selecting a range of optimal training days adds to the training process, as it allows to assess the robustness of selecting a short over a long (or medium) training window.

Taking all of the above into the consideration, a 5 day training window was selected for Explorer, and a 20 day window for second Wanderer mission.

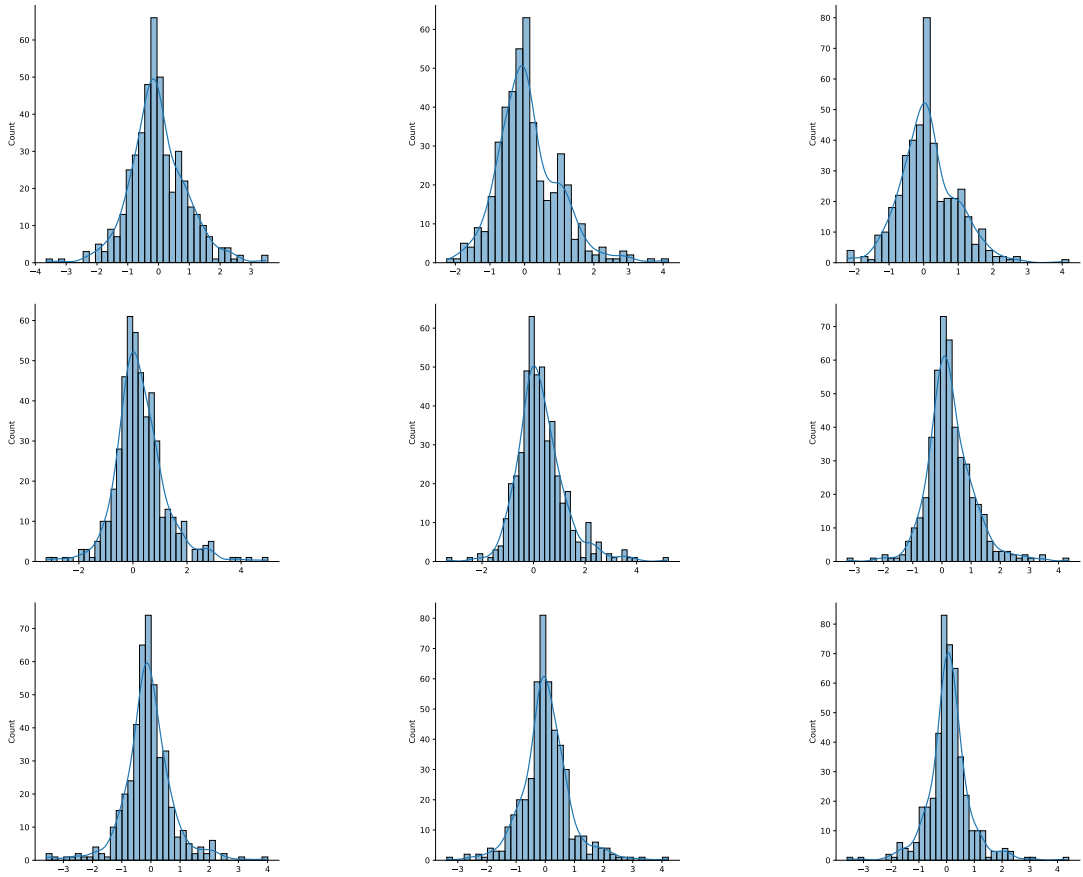


**Figure 25.** Histograms of the difference between the original forecast for Wanderer II mission versus the actual observed value. From top to bottom: DWD, WW3, MF; from left to right: 24H, 48H, 72H..

### **S3 Number of effective forecasts for Wanderer II and Explorer I missions**

In figure 38 authors present the number of effective forecasts for Explorer I and Wanderer II missions, similar to section 3.2. For the two missions same trend is visible - there are instances where only one forecast is an effective forecast in the overall ensemble. However, in the case of Explorer I mission two forecasts are leading number (50%) and three forecasts are effective in 25% of cases. During Wanderer II mission we see that it is between four and five forecast models are used mostly in the ensemble (40.7% and 28.8% of cases respectively). This figure 38 and the figure in the main body of the text support the authors hypothesis that the ensemble forecast made from more than one model is more effective in predicting short-term significant wave height than just one particular model.

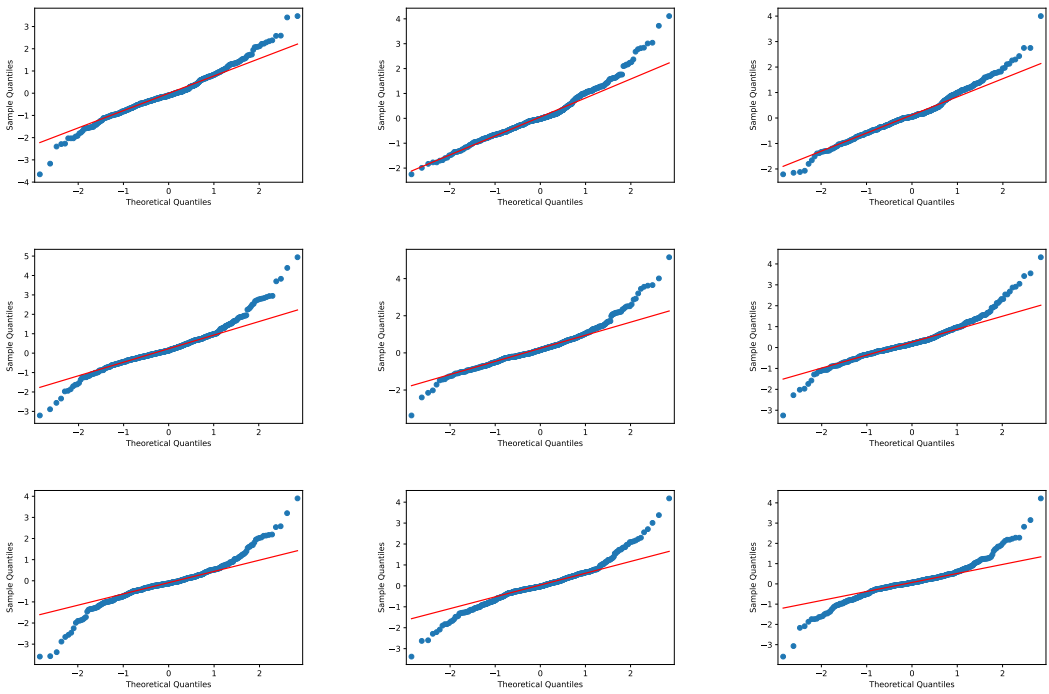


**Figure 26.** *Q-Q plots of the difference between the original forecast for Wanderer II mission versus the actual observed value. From top to bottom: DWD, WW3, MF; from left to right: 24H, 48H, 72H..*

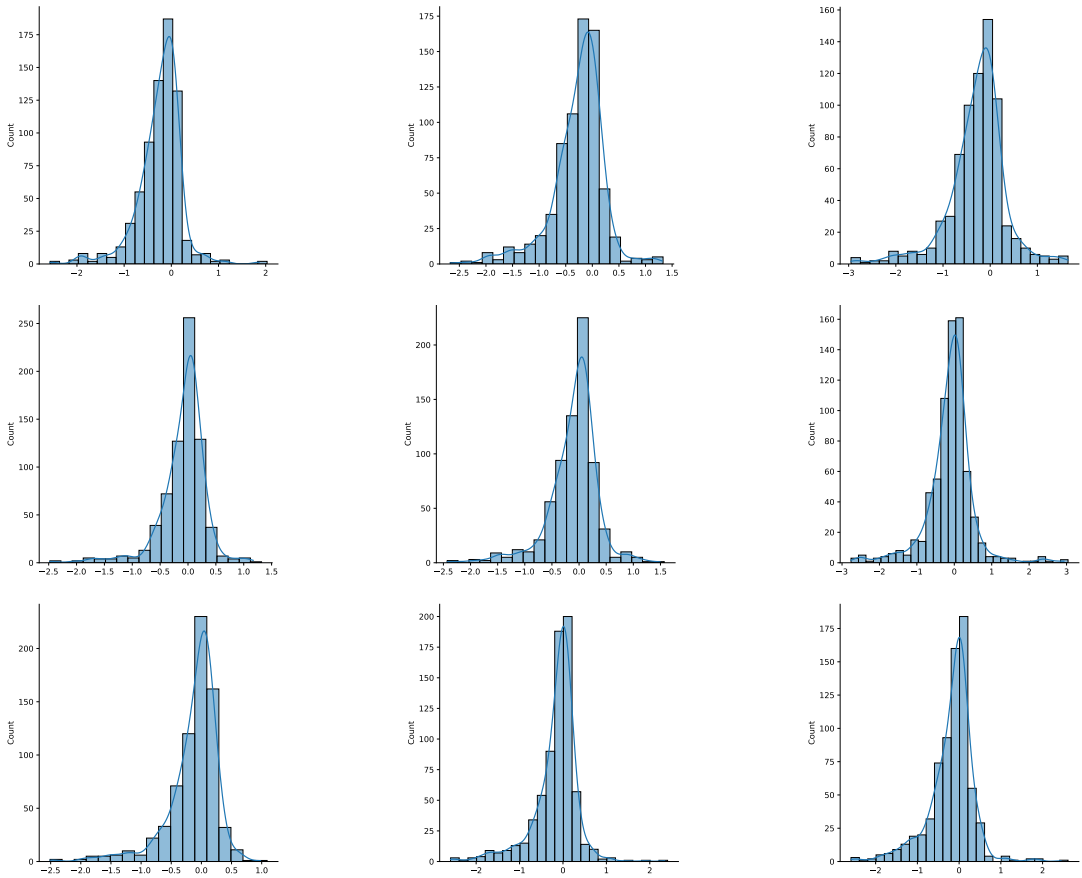


**Figure 27.** Histograms of the difference between the original forecast for Explorer I mission versus the actual observed value. From top to bottom: DWD, WW3, MF; from left to right: 24H, 48H, 72H..



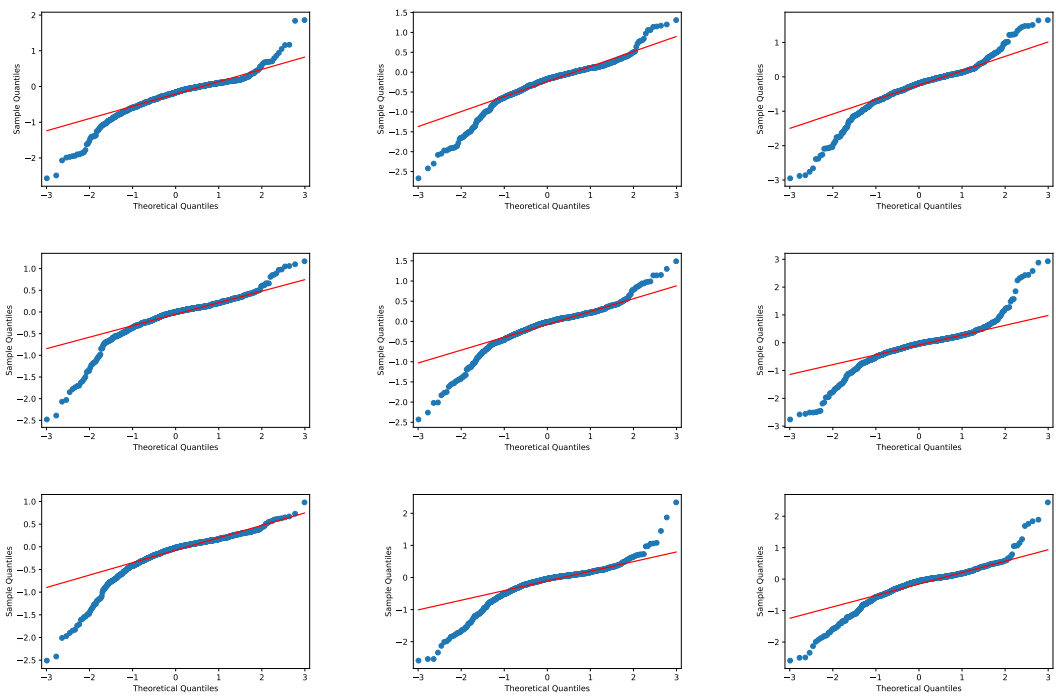


**Figure 28.** Q-Q plots of the difference between the original forecast for Explorer I mission versus the actual observed value. From top to bottom: DWD, WW3, MF; from left to right: 24H, 48H, 72H..

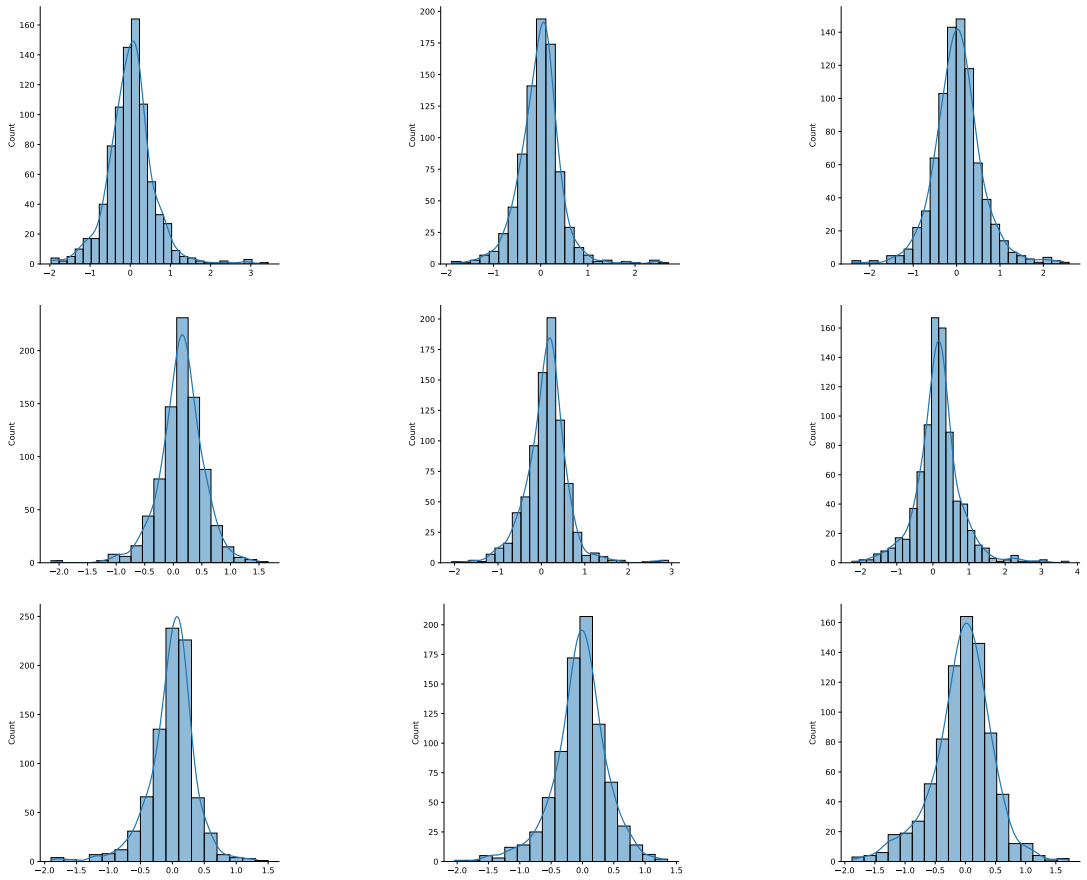


**Figure 29.** Histograms of the difference between the original forecast for M6 summer period versus the actual observed value. From top to bottom: DWD, WW3, MF; from left to right: 24H, 48H, 72H..

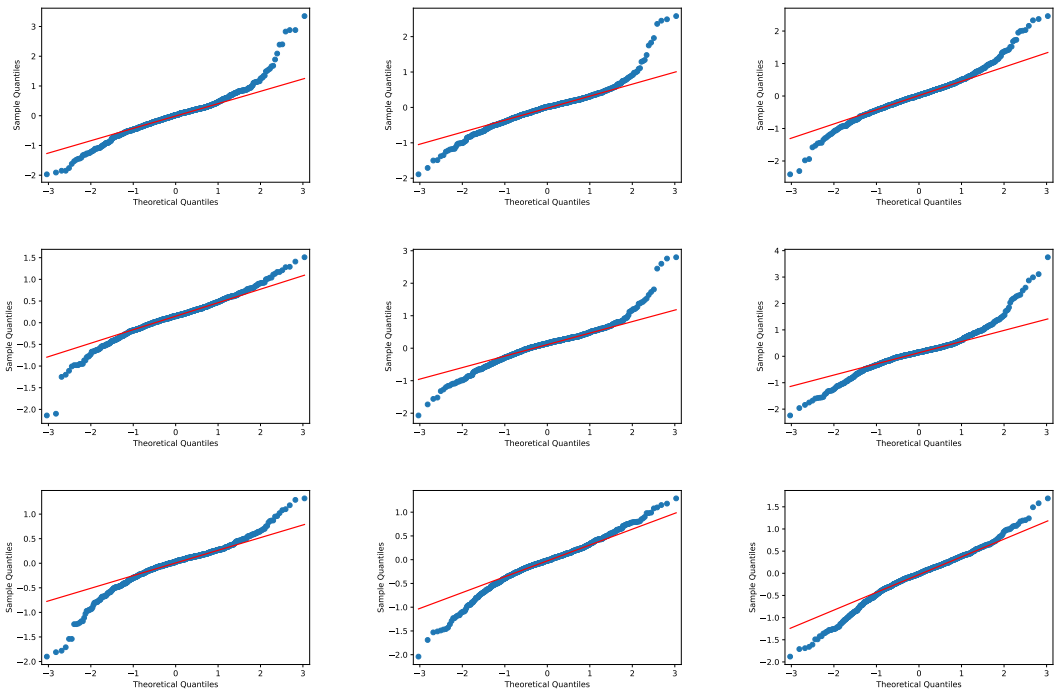


**Figure 30.** *Q-Q plots of the difference between the original forecast for M6 summer period versus the actual observed value. From top to bottom: DWD, WW3, MF; from left to right: 24H, 48H, 72H.*

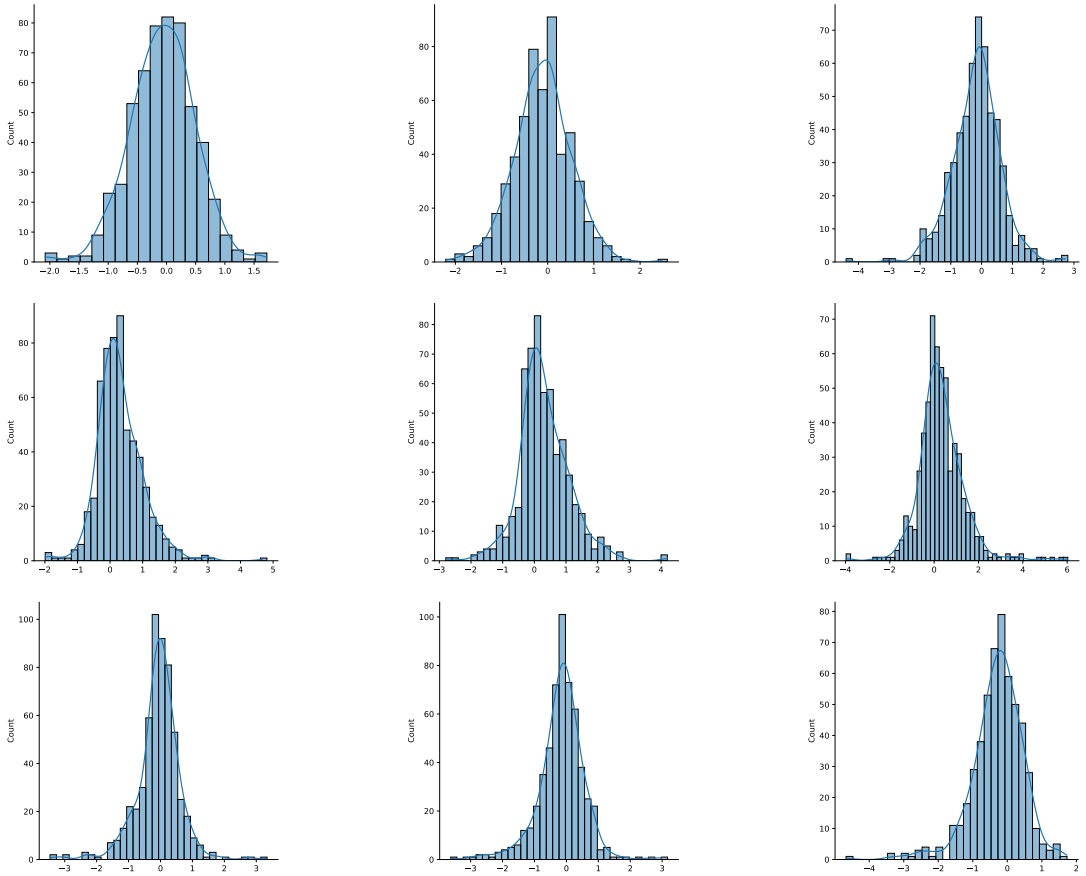


**Figure 31.** Histograms of the difference between the original forecast for M6 winter period versus the actual observed value. From top to bottom: DWD, WW3, MF; from left to right: 24H, 48H, 72H..

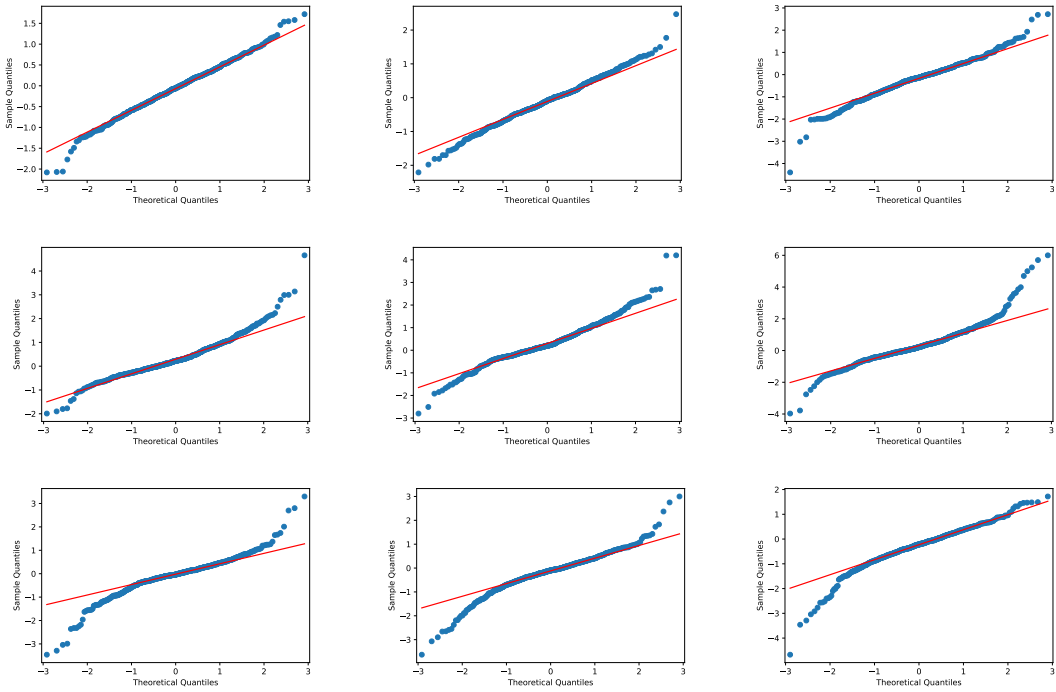


**Figure 32.** *Q-Q plots of the difference between the original forecast for M6 winter period versus the actual observed value. From top to bottom: DWD, WW3, MF; from left to right: 24H, 48H, 72H..*

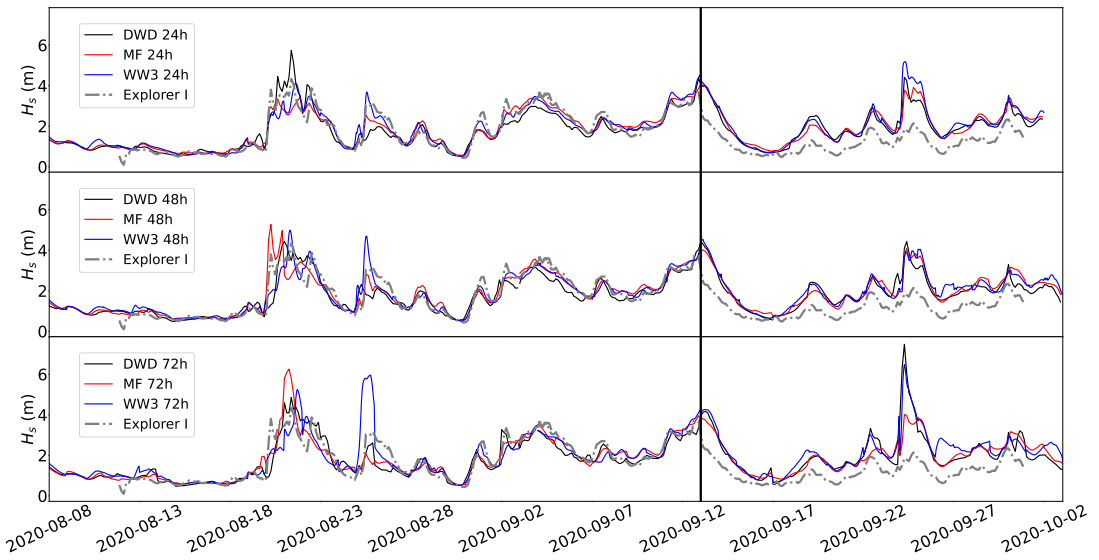


**Figure 33.** *Comparing actual  $H_s$  to the 24 hour (top), 48 hour (middle), and 72 hour (bottom) forecast  $H_s$  for the first Explorer mission. The vertical black line represents the time when Explorer started drifting. The discrepancy seen in the actual  $H_s$  recorded and the predicted  $H_s$  after that point is due to the Explorer drifting towards Connemara.*

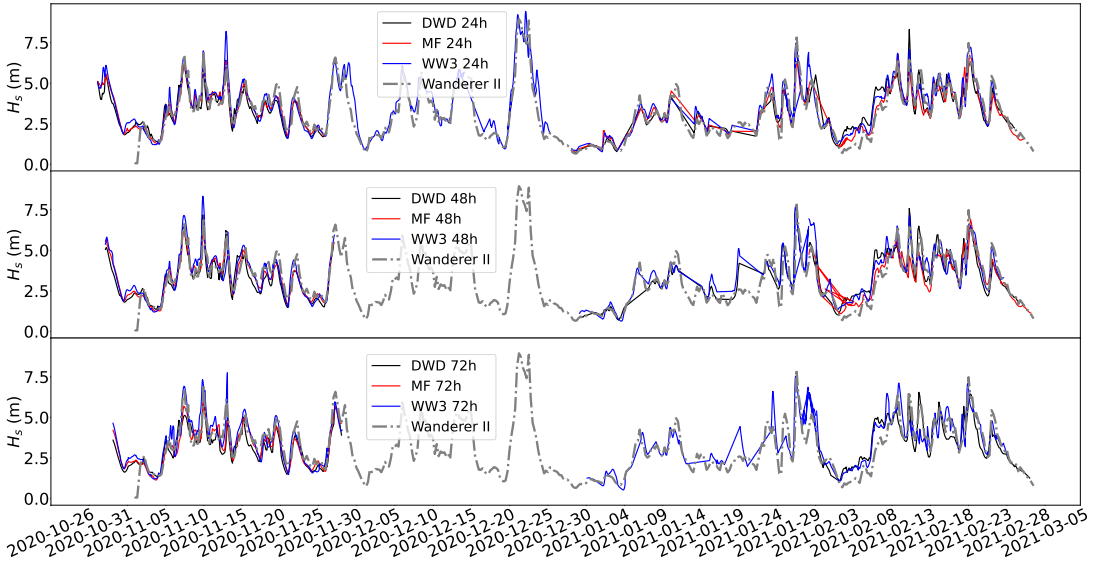


**Figure 34.** Comparing actual  $H_s$  to the 24 hour (top), 48 hour (middle), and 72 hour (bottom) forecast  $H_s$  for the second Wanderer mission. Note that during December 2020 - January 2021 there were new developments to the data collecting algorithms, hence the authors did not account for that data in the post-processing.

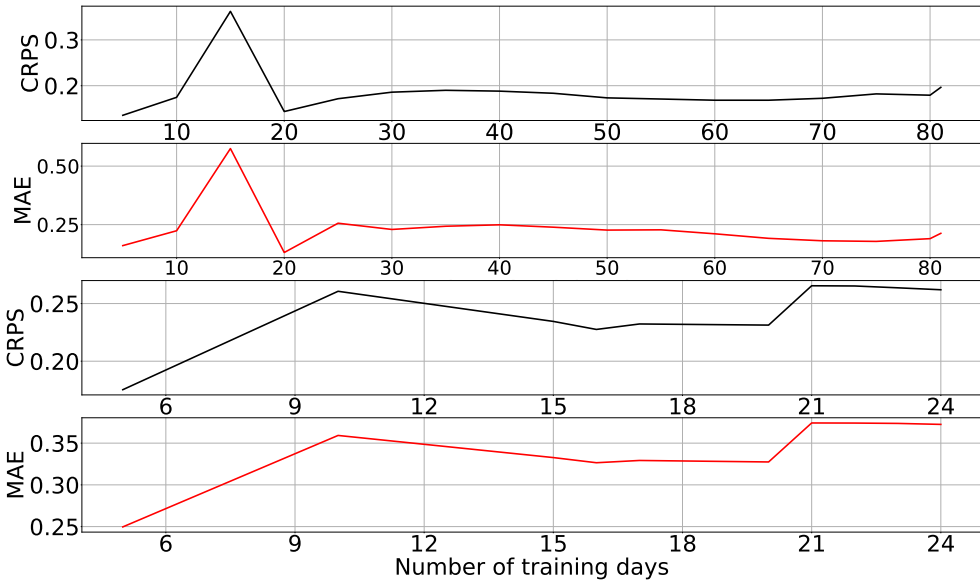


**Figure 35.** Comparison of second Wanderer mission (top panels) training period lengths for  $H_s$ : MAE (top, in meters), CRPS (bottom), and Explorer first mission (bottom panels)..

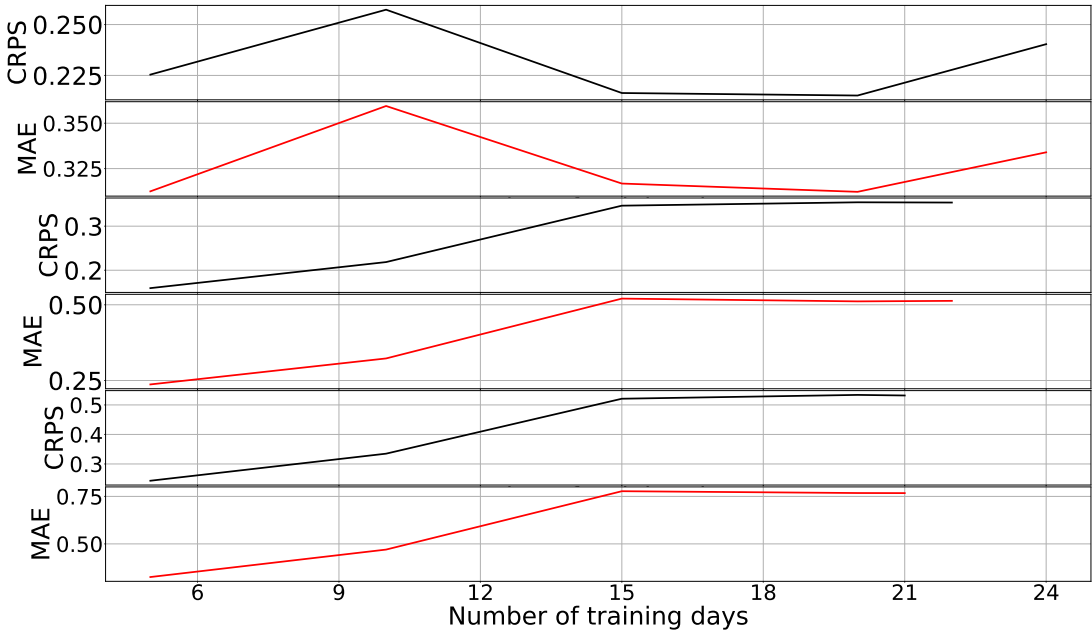


Figure 36. Comparison of Explorer 24H (top), 48H (middle), 72H (bottom) forecasts training period lengths for  $H_s$ : MAE (top, in meters), CRPS (bottom).

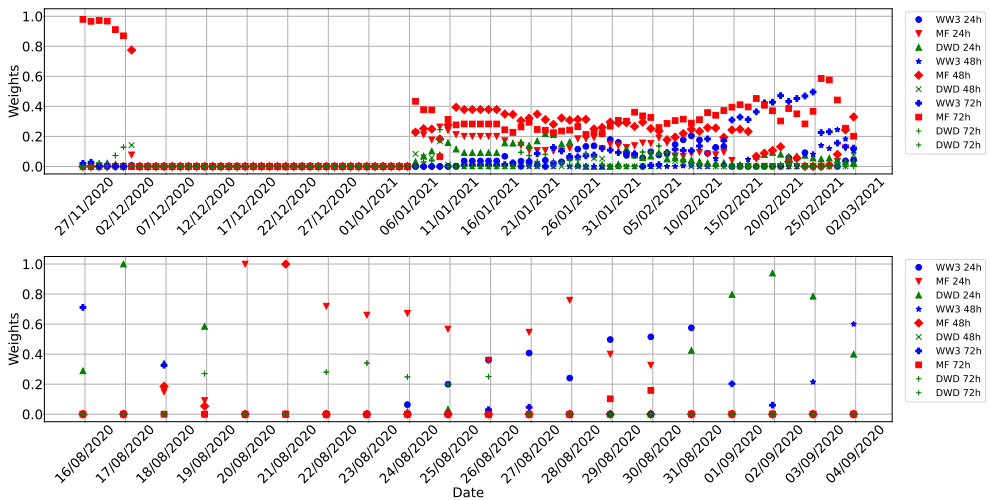
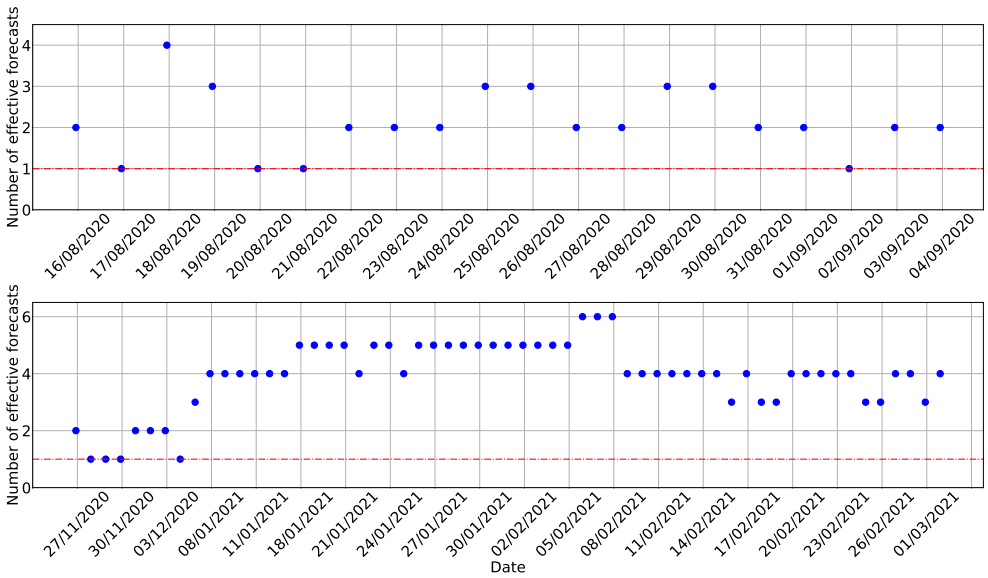


Figure 37. Wanderer II weights of individual forecast models. It is clearly visible, how MF is dominating the weight count towards the higher contribution to the ensemble forecast (top panel). Explorer I individual weights of every forecast contributing to the overall trained prediction. We see how with time, the higher contributor changes. For example, we see MF dominating between 20 August and 28 August, and then WW3 taking over for three days, followed by DWD (bottom panel).



**Figure 38.** Explorer I number of effective forecasts (top panel). Wanderer II number of effective forecasts (bottom panel)..